# Homogeneous Catalytic Carbonylation of Nitroaromatics. 5. Kinetics and Mechanism of Aniline and Carbamate Formation Using $Ru(Ph_2PCH_2CH_2PPh_2)(CO)_3$

**Jerry D. Gargulak, Amanda J. Berry, Mark D. Noirot, and Wayne L. Gladfelter***

*Contribution from the Department of Chemistry, University of Minnesota, Minneapolis, Minnesota 55455.* *Received February 20, 1992*

**Abstract:** Kinetic and mechanistic studies of the catalytic conversion of nitroaromatics and methanol to methyl *N*-arylcarbamates utilizing elevated pressures of CO, elevated temperatures, and the presence of a homogeneous catalyst, $Ru(dppe)(CO)_3$ where dppe = 1,2-bis(diphenylphosphino)ethane, are described. The kinetics were studied in *o*-xylene over a range of CO pressures (22–103 atm), temperatures (125–155 °C), catalyst concentrations (1.3–11.2 mM), methanol concentrations (1.2–24.7 M), and initial aniline concentrations (2.2–52 mM). Aniline was confirmed to be a byproduct of the reaction as well as an intermediate in the formation of carbamate. Aniline formation was first order in catalyst concentration and inverse first order with respect to the pressure of CO. The rate of carbamate formation was first order in both catalyst concentration and aniline concentration. The integrated kinetic model gave good fits to the data over the above range of parameters. Stoichiometric reactions established that the catalytic cycle can be separated into three distinct segments each occurring with an increasing kinetic barrier. Phase 1, which occurs at room temperature, involves the reaction of $Ru(dppe)(CO)_3$ with $ArNO_2$ and CO to give the unusual complex $Ru(dppe)(CO)_2[C(O)N(Ar)O]$ which was characterized using solution spectroscopic and, for Ar = *p*-chlorophenyl, X-ray crystallographic methods [triclinic crystal system, $P\bar{1}$ space group, $a$ = 9.372 (5) Å, $b$ = 10.59 (2) Å, $c$ = 17.24 (1) Å, $\alpha$ = 102.0 (1)°, $\beta$ = 104.40 (4)°, $\gamma$ = 100.46 (9)°, $V$ = 1572 (6), $Z$ = 2]. Phase 2 involves the reaction of $Ru(dppe)(CO)_2[C(O)N(Ar)O]$ with methanol and CO. Aniline and $CO_2$ are released, and the new bis(methoxycarbonyl) complex, $Ru(dppe)(CO)_2[C(O)OMe]_2$, was isolated in high yield. This reaction proceeds through an intermediate identified as the bis(methanolato) complex, $Ru(dppe)(CO)_2(OMe)_2$. Carbamate formation occurs during Phase 3 of the catalysis and involves the reaction of $ArNH_2$ with $Ru(dppe)(CO)_2[C(O)OMe]_2$. Both in situ infrared spectroscopy and $^{31}P$ NMR spectroscopy of rapidly quenched samples withdrawn from the catalytic solutions establish that $Ru(dppe)(CO)_2[C(O)OMe]_2$ is the major species present during the catalysis. Details of the proposed mechanism of the catalysis are discussed along with comments relating these results to other catalytic systems.

## Introduction

Aromatic isocyanates such as 2,4-diisocyanatotoluene (TDI) and 4,4′-bis(phenylisocyanato)methane (MDI) are used on a large scale for the production of polyurethanes. The starting materials

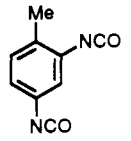

TDI

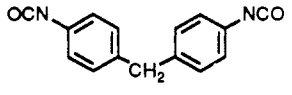

MDI

for aryl isocyanates are the corresponding nitro compounds, which are catalytically hydrogenated into an amine and subsequently reacted with phosgene ($Cl_2CO$). Although this two-step synthesis proceeds in high yields, there has long been interest in developing routes that bypass the phosgene step.[1]

Numerous patents[2-6] and publications[7-10] describe the catalytic carbonylation of nitroaromatics directly to isocyanates (eq 1), but the lifetimes for most of these are low. In addition, even those

$$ArNO_2 + 3CO \rightarrow ArNCO + 2CO_2 \quad (1)$$

catalytic systems which show promise for the carbonylation of nitrobenzene fail to carbonylate fully 2,4-dinitrotoluene and related species.[1]

Recent attention has focused on the modification involving the addition of alcohol, especially methanol, to the reaction (eq 2).[11-18] The product is a carbamate which can be converted into the

$$ArNO_2 + 3CO + MeOH \rightarrow ArNHC(O)OMe + 2CO_2 \quad (2)$$

arylisocyanate by removing the methanol at elevated temperatures. Both of the successful catalytic systems for eq 2 utilize a ruthenium carbonyl, e.g. $Ru(PPh_3)_2(CO)_3$ or $Ru_3(CO)_{12}$, as the catalyst and are conducted at pressures of approximately 60 atm and temperatures near 150 °C. Cenini and co-workers discovered that the presence of a tetraalkylammonium chloride cocatalyst vastly improves the efficiency of the reaction.[15,16,19,20] Grate and co-workers studied the effect of adding arylamine to the reaction and found that both the selectivity and the rate of the catalysis are dramatically improved.[11-14] The complex containing the chelating diphosphine ligand, 1,2-bis(diphenylphosphino)ethane (dppe), was reported to be the most active catalyst under conditions explored by Grate and co-workers.[12]

In addition to studies of the actual catalytic systems, several reports of the chemistry of ruthenium carbonyl clusters containing arylimido ligands formed from a nitro- or nitrosoaromatic have

(1) Cenini, S.; Pizzotti, M.; Crotti, C. In *Aspects of Homogeneous Catalysis*; Ugo, R., Ed.; Reidel: Dordrecht, 1988; Vol. 6, pp 97–198.
(2) Smith, E. M., German Patent 1,957,965, 1970.
(3) Mizoguchi, Y.; Ono, S.; Iwaisako, T. Japan Patent 74,92,041, 1975.
(4) Balabanov, G. P.; Dergunov, Y. I.; Khoshdurdyev, K. O.; Manov-Yuvenskii, V. I.; Neredov, B. K.; Rysikhin, A. I. U.S. Patent 4,207,212, 1980.
(5) Cognion, J. M.; Kervennal, J. Eur. Patent 4,224, 1980.
(6) Bhaduri, S. U.S. Patent 4,491,670, 1985.
(7) Braunstein, P.; Bender, R.; Kervennal, J. *Organometallics* **1982**, *1*, 1236.
(8) Gupte, S. P.; Chaudhari, R. V. *J. Mol. Catal.* **1984**, *24*, 197.
(9) Ugo, R.; Psaro, R.; Pizzotti, M.; Nardi, P.; Dossi, C.; Andreetta, A.; Capparella, G. *J. J. Organomet. Chem.* **1991**, *417*, 211.
(10) Cenini, S.; Ragaini, F.; Pizzotti, M.; Porta, F.; Mestroni, G.; Alessio, E. *J. Mol. Catal.* **1991**, *64*, 179.
(11) Grate, J. H.; Hamm, D. R.; Valentine, D. H. U.S. Patent 4,600,793, 1986.
(12) Grate, J. H.; Hamm, D. R.; Valentine, D. H. U.S. Patent 4,603,216, 1986.
(13) Grate, J. H.; Hamm, D. R.; Valentine, D. H. U.S. Patent 4,629,804, 1986.
(14) Grate, J. H.; Hamm, D. R.; Valentine, D. H. U.S. Patent 4,705,883, 1987.
(15) Cenini, S.; Pizzotti, M.; Crotti, C.; Porta, F.; La Monica, G. *J. Chem. Soc., Chem. Commun.* **1984**, 1286.
(16) Cenini, S.; Crotti, C.; Pizzotti, M.; Porta, F. *J. Org. Chem.* **1988**, *53*, 1243.
(17) Kahn, M. M. T.; Halligudi, S. B.; Shukla, S.; Shaikh, Z. A. *J. Mol. Catal.* **1990**, *57*, 307–312.
(18) Bhaduri, S.; Sharma, K. R.; Khwaja, H. I. *Proc. Indian Acad. Sci. (Chem. Sci.)* **1989**, *101*, 195.
(19) Cenini, S.; Pizzotti, M.; Crotti, C.; Porta, F. Italian Patent 21951A/83, 1983.
(20) Cenini, S.; Pizzotti, M.; Crotti, C.; Porta, F. Italian Patent 22632A/85, 1985.

0002-7863/92/1514-8933$03.00/0 

appeared.[21-33] These studies have always been considered relevant to the nitroaromatic carbonylation because arylimido (nitrene) ligands have been viewed as playing a central role in the catalytic chemistry. Examples of mono-[34,35] and dinuclear[36-39] low-valent complexes of the late transition elements containing arylimido ligands have been reported recently. Although these isolated mono- and polynuclear arylimido complexes undergo chemical reactions related to the catalysis, no quantitative results have yet tied them to an actual catalytic cycle. Further, no experimental details have appeared establishing how the nitroaromatic interacts with the catalyst and how the N–O bonds are cleaved. In addition to addressing these questions, we sought to understand the critical role that methanol plays and why the addition of excess aniline to the system improves the selectivity. Our first study has focused on $Ru(dppe)(CO)_3$, I, because (a) it has high activity, (b) the

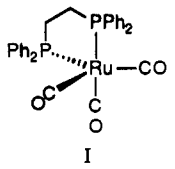

I

chelating diphosphine was expected to inhibit cluster formation, and (c) the dppe ligand itself would provide a structure-sensitive spectroscopic probe. Preliminary reports of part of this research have appeared.[40,41]

## Experimental Section

**General.** Standard Schlenk techniques were implemented when working with all organometallic compounds. A nitrogen-filled Vacuum Atmospheres drybox equipped with a Dri-Train Model 40-1 inert gas purifier was employed for manipulations carried out under glovebox conditions. $Ru_3(CO)_{12}$ was purchased from Strem Chemical and was recrystallized from methanol. Sodium nitrite-$^{15}N$ was purchased from MSD Isotopes. *o*-Bromotoluene, carbon monoxide-$^{13}C$, 1.0 M HCl in diethyl ether, 1,2-bis(diphenylphosphino)ethane, methanol-$^{13}C$, methanol-$d_4$, benzene-$d_6$, *p*-nitrotoluene, *p*-chloronitrobenzene, *o*-nitrotoluene, and *p*-tolylisocyanate were purchased from Aldrich Chemical Co. 1,2-Bis(diphenylphosphino)ethane was subsequently purified by recrystallization from hexane/toluene. *p*-Nitrotoluene was dissolved in toluene and the solution was dried with magnesium sulfate prior to recrystallization under a nitrogen atmosphere by addition of hexane. Benzene-$d_6$ was distilled from $LiAlH_4$. Methanol was doubly distilled from $CaH_2$. The kinetic experiments utilized anhydrous methanol packed under nitrogen available from Aldrich Chemical Co. $Ru(dppe)(CO)_3$ was prepared using literature methods.[42] Carbon monoxide (CP grade) was purchased from Matheson and used as received. *o*-Xylene, toluene, diethyl ether, and hexane were distilled from sodium or potassium under prepurified nitrogen.

All in situ high-pressure FTIR spectra were obtained using a CIR FTIR cell[43] and bench manufactured by Spectra Tech and mounted on a Mattson Sirius 100 spectrometer. The crystal used for these experiments was silicon. Routine infrared spectra were collected on a Mattson Cygnus 25 spectrometer. The $^1H$, $^{13}C$, and $^{31}P$ NMR studies were performed using a Varian Unity 300-MHz spectrometer. Nitrogen-15 NMR spectroscopy was performed using a Nicolet 300-MHz spectrometer. Solution gas chromatography samples were analyzed on an HP 5890 series II employing a 10-m megabor FFAP cross-linked column and flame ionization detector. Headspace analysis was performed using a Varian Model 3700 gas chromatograph equipped with a 8-ft carbosphere column and a thermal conductivity detector.

**Synthesis of Ru(dppe)(CO)$_2$[C(O)N(Ar)O] (Ar = *o*-Tolyl; IIa).** To a 20-mL vial containing $Ru(dppe)(CO)_3$ (1.0 g, 1.72 mmol) and dry degassed toluene (7.0 mL) under nitrogen atmosphere was added through a septum 7.0 mL of a 246 mM solution of *o*-nitrosotoluene in toluene. After 5 h at ambient temperature the yellow microcrystalline product was collected on a Schlenk frit, washed twice with dry hexane, and dried in vacuo to yield 1.13 g of $Ru(dppe)(CO)_2[C(O)N(o\text{-tolyl})O]$ (93% yield). IR ($cm^{-1}$, $CH_2Cl_2$): 2047 (s), 1972 (s), 1611 (m). $^1H$ NMR (ppm, $CD_2Cl_2$): 2.31 (s, $CH_3$), 2.48 (m, $CH_2$), 2.83 (m, $CH_2$), 6.14 (d, $J_{AB}$ = 7.8 Hz, H(A)), 6.74 (t, $J_{AB,BC}$ = 7.5 Hz, H(B)), 6.85 (t, $J_{CB,CD}$ = 7.4 Hz, H(C)), 6.98 (d, $J_{DC}$ = 7.4 Hz, H(D)). $^{31}P$ NMR (ppm, $CD_2Cl_2$): 46.7 (d, $J_{PP}$ = 12.3 Hz), 47.1 (d, $J_{PP}$ = 12.6 Hz). $^{13}C$ NMR (ppm, $CD_2Cl_2$): 19.7 (s, $CH_3$), 26.67 (dd, $J_{CP1}$ = 19.6 Hz, $J_{CP2}$ = 29 Hz, $CH_2$), 28.12 (dd, $J_{CP1}$ = 12.3 Hz, $J_{CP2}$ = 26.8 Hz, $CH_2$), 183.58 (dd, $J_{CP1}$ = 11.15 Hz, $J_{CP2}$ = 82 Hz, CO), 196.60 (dd, $J_{CP1}$ = 7.39 Hz, $J_{CP2}$ = 97.4 Hz, CO), 196.91 (dd, $J_{CP1}$ = 5.44 Hz, $J_{CP2}$ = 13.3 Hz, CO). Anal. Calcd for $Ru(dppe)(CO)_3(NOC_6H_4CH_3)$: C, 61.84; H, 4.62; N, 1.95; P, 8.62. Found: C, 61.76; H, 4.65; N, 1.94; P, 8.39. Mass spectrum ($Ru^{102}$) P (*m/e*): 706.

**Preparation of *o*-Nitrosotoluene-$^{15}N$.** The following procedure was adapted from the literature.[44] $Na^{15}NO_2$ (0.415 g, 5.93 mmol) was dissolved in water (3 mL) and added dropwise over 10 min using an addition funnel to a three-necked 50.0-mL round-bottomed flask containing 5 mL of concentrated HCl. The $^{15}NOCl$ was sublimed as a yellow crystalline solid into a 50-mL Schlenk tube cooled with dry ice/acetone and connected to the three-necked flask via a distillation head. The resulting solid $^{15}NOCl$ (0.253 g, 3.8 mmol, 64% yield) was placed in a 50-mL Schlenk tube under nitrogen atmosphere and dissolved in methylene chloride (5 mL). *o*-Tolyltrimethyltin (0.945 g, 3.7 mmol) was dissolved in methylene chloride (5 mL), placed in an addition funnel under nitrogen, and added over 20 min to the solution of $^{15}NOCl$ held at −21 °C. The solution was warmed to 0 °C and held at this temperature for 2 h. The green solution was washed once with 0.01 M KOH and twice with $H_2O$, dried over $MgSO_4$, filtered, and concentrated to yield green crystalline $o\text{-}CH_3C_6H_4{}^{15}NO$ (0.30 g, 2.46 mmol, 41% yield overall).

**Synthesis and Spectroscopy of Ru(dppe)(CO)$_2$[C(O)$^{15}$N-(*o*-tolyl)O].** $Ru(dppe)(CO)_3$ (0.126 g, 0.215 mmol) was dissolved in 5 mL of toluene, and the resulting solution was filtered into a 50-mL round-bottomed flask purged with $N_2$. In a 10-mL vial, *o*-nitrosotoluene-$^{15}N$ (28 mg, 0.230 mmol) was dissolved in 3 mL of toluene, purged with $N_2$, and transferred to a small addition funnel under $N_2$ atmosphere. This solution was added dropwise to the $Ru(dppe)(CO)_3$ over a 60-min period with occasional agitation. After 2.5 h the yellow microcrystalline product was filtered using a Schlenk frit, washed with two 10-mL portions of hexane, and dried in vacuo. IR ($cm^{-1}$, $CH_2Cl_2$): 2048 (s), 1972 (s), 1615 (m). $^1H$ NMR (ppm, $CD_2Cl_2$): 2.31 (s, $CH_3$), 2.48 (m, $CH_2$), 2.83 (m, $CH_2$), 6.14 (d, $J_{AB}$ = 7.8 Hz, H(A)), 6.74 (t, $J_{AB,BC}$ = 7.5 Hz, H(B)), 6.85 (t, $J_{CB,CD}$ = 7.4 Hz, H(C)), 6.98 (d, $J_{DC}$ = 7.4 Hz, H(D)). $^{31}P$ NMR (ppm, $CD_2Cl_2$): 46.7 (t, $J_{PN}$ = 13.2 Hz, $J_{PP}$ = 12.8 Hz), 48.7 (d, $J_{PP}$ = 12.8 Hz). $^{13}C$ NMR (ppm, $CD_2Cl_2$): 19.7 (s, $CH_3$), 26.7 (dd, $J_{CP1}$ = 19.6 Hz, $J_{CP2}$ = 29 Hz, $CH_2$), 28.12 (dd, $J_{CP1}$ = 12.3 Hz, $J_{CP2}$ = 26.8 Hz, $CH_2$), 183.9 (dd, $J_{CP1}$ = 11.2, $J_{CP2}$ = 82.0 Hz, CO), 196.6 (dd, $J_{CP1}$ = 7.39 Hz, $J_{CP2}$ = 97.4 Hz, CO), 196.9 (dd, $J_{CP1}$ = 5.44 Hz, $J_{CP2}$ = 13.3

(21) Sappa, E.; Milone, L. *J. Organomet. Chem.* **1973**, *61*, 383.
(22) Bhaduri, S.; Gopalkrishnan, K. S.; Sheldrick, G. M.; Clegg, W.; Stalke, D. *J. Chem. Soc., Dalton Trans.* **1983**, 2339.
(23) Bhaduri, S.; Gopalkrishnan, K. S.; Clegg, W.; Jones, P. G.; Sheldrick, G. M.; Stalke, D. *J. Chem. Soc., Dalton Trans.* **1984**, 1765.
(24) Clegg, W.; Sheldrick, G. M.; Stalke, D.; Bhaduri, S.; Gopalkrishnan, K. S. *Acta Crystallogr., Sect. C: Cryst. Struct. Commun.* **1984**, *C40*, 927.
(25) Smieja, J. A.; Gladfelter, W. L. *Inorg. Chem.* **1986**, *25*, 2667.
(26) Basu, A.; Bhaduri, S.; Khwaja, H. *J. Organomet. Chem.* **1987**, *319*, C28.
(27) Han, S.-H.; Geoffroy, G. L.; Rheingold, A. L. *Inorg. Chem.* **1987**, *26*, 3426.
(28) Han, S.-H.; Geoffroy, G. L. *Polyhedron* **1988**, *7*, 2331.
(29) Bhaduri, S.; Khwaja, H.; Jones, P. G. *J. Chem. Soc., Chem. Commun.* **1988**, 194.
(30) Bhaduri, S.; Khwaja, H.; Sharma, K.; Jones, P. G. *J. Chem. Soc., Chem. Commun.* **1989**, 515.
(31) Song, J.-S.; Han, S.-H.; Nguyen, S. T.; Geoffroy, G. L.; Rheingold, A. L. *Organometallics* **1990**, *9*, 2386.
(32) Bhaduri, S.; Khwaja, H.; Sapre, N.; Sharma, K.; Basu, A.; Jones, P. G.; Carpenter, G. *J. Chem. Soc., Dalton Trans.* **1990**, 1313.
(33) Crotti, C.; Cenini, S.; Bassoli, A.; Rindone, B.; Demartin, F. *J. Mol. Catal.* **1991**, *70*, 175.
(34) Glueck, D. S.; Hollander, F. J.; Bergman, R. G. *J. Am. Chem. Soc.* **1989**, *111*, 2719.
(35) Glueck, D. S.; Wu, J.; Hollander, F. J.; Bergman, R. G. *J. Am. Chem. Soc.* **1991**, *113*, 2041.
(36) Sharp, P. R.; Ge, Y.-W. *J. Am. Chem. Soc.* **1987**, *109*, 3796.
(37) Ge, Y.-W.; Sharp, P. R. *Organometallics* **1988**, *7*, 2234.
(38) Ge, U. W.; Peng, F.; Sharp, P. R. *J. Am. Chem. Soc.* **1990**, *112*, 2632.
(39) Ge, Y.-W.; Sharp, P. R. *Inorg. Chem.* **1992**, *31*, 379.
(40) Kunin, A. J.; Noirot, M. D.; Gladfelter, W. L. *J. Am. Chem. Soc.* **1989**, *111*, 2739.
(41) Gargulak, J. D.; Noirot, M. D.; Gladfelter, W. L. *J. Am. Chem. Soc.* **1991**, *113*, 1054.
(42) Sanchez-Delgado, R. A.; Bradley, J. S.; Wilkinson, G. *J. Chem. Soc., Dalton Trans.* **1976**, 399–404.
(43) Moser, W. R.; Cnossen, J. E.; Wang, A. W.; Krouse, S. A. *J. Catal.* **1985**, *95*, 21.
(44) Eaborn, C.; Hornfeld, H. L.; Walton, D. R. M. *J. Organomet. Chem.* **1967**, *10*, 529–530.

**Table I.** Summary of Crystallographic Data

| | |
|---|---|
| **Crystal Parameters** | |
| compound | $Ru(dppe)(CO)_2]C(O)N(ClC_6H_4)O]$ |
| crystal system | triclinic |
| space group | $P\bar{1}$ |
| formula | $RuC_{35}H_{28}P_2O_4NCl$ |
| formula weight, g mol$^{-1}$ | 725.10 |
| $a$, Å | 9.372 (5) |
| $b$, Å | 10.59 (2) |
| $c$, Å | 17.24 (1) |
| $a$, deg | 102.0 (1) |
| $\beta$, deg | 104.40 (4) |
| $\gamma$, deg | 100.46 (9) |
| $V$, Å$^3$ | 1572 (6) |
| $Z$ | 2 |
| $\rho$(calcd), g cm$^{-3}$ | 1.534 |
| temp, °C | 24 (2) |
| abs coeff, cm$^{-1}$ | 7.13 |
| crystal dimens, mm | 0.60 × 0.40 × 0.20 |
| trans. factors, max to min % | 118 to 72 |
| abs corr applied | empirical |
| **Measurement of Intensity Data** | |
| diffractometer | Enraf-Nonius CAD-4 |
| radiation | Mo K$\alpha$ ($\lambda$ = 0.71073 Å) |
| monochromator | graphite crystal |
| programs used | TEXSAN |
| method of structure soln | Patterson method |
| scan type | $\omega$–$2\theta$ |
| scan range, deg | 0–51.9 |
| reflcns meas | $h,\pm k,\pm l$ |
| no. of unique reflcns | 6169 |
| no. of reflcns used | 4818 |
| cutoff | $3\sigma$ |
| $p$ | 0.05 |
| $R$ | 0.049 |
| $R_w$ | 0.065 |
| error in observation of unit weight | 1.88 |

Hz, CO). $^{15}N$ NMR (ppm, $CD_2Cl_2$, referenced to nitromethane): −142.0 (d, $J_{NP}$ = 14.6 Hz).

**Quantitation of $CO_2$ Evolved from the Stoichiometric Reaction of Ru(dppe)(CO)$_3$ and *p*-Chloronitrobenzene.** A 15-mL vial was loaded with $Ru(dppe)(CO)_3$ (0.0505 g, 0.0865 mmol) and sealed with a septum and 2.0 mL of *o*-xylene–methanol (5:1) solvent was added. The vial was purged with dry CO gas, and then 1.0 mL of methane was injected into the vial using a gastight syringe for use as an internal standard. A 50-$\mu$L sample of the headspace was removed from the vial using a gastight syringe after 2 min and analyzed by GC. The reaction was started by injecting 1.0 mL of a 90.7 mM solution of *p*-chloronitrobenzene into the vial. Gas samples (50 $\mu$L) were removed periodically while the vial was held at ambient temperature. A similar procedure was used to quantify gas evolution and uptake in other stoichiometric reactions.

**X-ray Crystallography of Ru(dppe)(CO)$_2$[C(O)N(*p*-chlorophenyl)O].** Yellow prisms were grown from toluene and one of these was mounted on a glass fiber. Table I includes the details of the structural analysis. A preliminary peak search of 25 centered reflections ($12° < 2\theta < 38.2°$) indicated that the crystal was triclinic. Despite attempts to minimize the relatively large deviations of the cell constants, no improvement was found. The TEXSAN programs used for the least-squares refinement incorporated the estimated standard deviations of the cell parameters in the calculation of the errors in bond distances and angles. The centric space group $P\bar{1}$ (No. 2) was chosen and led to successful refinement of the structure. During data collection, no decay of intensity was observed in three check reflections measured every 50 min. All non-hydrogen atoms were refined anisotropically. Hydrogen atoms were included in the structure factor calculation in idealized positions with $d_{C-H}$ = 0.95 Å and an isotropic temperature factor 20% greater than the $B_{eq}$ of the carbon to which they were bonded. The maximum and minimum peaks on the final difference Fourier map corresponded to +1.11 and −1.35 e/Å$^3$, respectively. The values of the atomic scattering factors used in the calculations were taken from the usual tabulations, and the effects for anomalous dispersion were included for the non-hydrogen atoms.[45-47]

(45) Cromer, D. T.; Waber, J. T. In Kynoch Press: Birmingham, England, 1974; Vol. IV, Table 2.2A.
(46) Cromer, D. T. In Kynoch Press: Birmingham, England, 1974; Vol. IV, Table 2.3.1.

**Table II.** Bond Distances (Å) in Ru(dppe)(CO)$_2$[C(O)N(*p*-chlorophenyl)O]

| | | | |
|---|---|---|---|
| **A. Metal–Ligand Distances** | | | |
| Ru1–P1 | 2.388 (2) | Ru1–P2 | 2.377 (4) |
| Ru1–O1 | 2.104 (5) | Ru1–C3 | 2.081 (5) |
| Ru1–C4 | 1.913 (6) | Ru1–C5 | 1.855 (6) |
| **B. Intraligand Distances** | | | |
| P1–C21 | 1.813 (6) | P1–C11 | 1.822 (5) |
| P1–C1 | 1.826 (6) | P2–C31 | 1.817 (6) |
| P2–C41 | 1.818 (6) | P2–C2 | 1.832 (5) |
| O1–N1 | 1.414 (5) | O3–C3 | 1.239 (6) |
| O4–C4 | 1.143 (7) | O5–C5 | 1.148 (7) |
| N1–C3 | 1.353 (7) | N1–C51 | 1.388 (7) |
| C1–C2 | 1.541 (8) | C11–C12 | 1.365 (8) |
| C11–C16 | 1.392 (7) | C12–C13 | 1.396 (8) |
| C13–C14 | 1.36 (1) | C14–C15 | 1.37 (1) |
| C15–C16 | 1.383 (8) | C21–C26 | 1.374 (8) |
| C21–C22 | 1.395 (8) | C22–C23 | 1.38 (1) |
| C23–C24 | 1.39 (1) | C24–C25 | 1.37 (1) |
| C25–C26 | 1.39 (1) | C31–C36 | 1.378 (9) |
| C31–C32 | 1.402 (8) | C32–C33 | 1.39 (1) |
| C33–C34 | 1.38 (1) | C34–C35 | 1.36 (1) |
| C35–C36 | 1.39 (1) | C41–C46 | 1.382 (8) |
| C41–C42 | 1.392 (8) | C42–C43 | 1.40 (1) |
| C43–C44 | 1.39 (1) | C44–C45 | 1.37 (1) |
| C45–C46 | 1.39 (1) | C51–C56 | 1.380 (8) |
| C51–C52 | 1.409 (7) | C52–C53 | 1.381 (9) |
| C53–C54 | 1.369 (9) | C54–C55 | 1.373 (8) |
| C55–C56 | 1.395 (9) | CL1–C54 | 1.751 (7) |

**Table III.** Bond Angles for Ru(dppe)(CO)$_2$[C(O)N(*p*-chlorophenyl)O]

| | | | |
|---|---|---|---|
| **A. Ligand–Metal–Ligand** | | | |
| C5–Ru1–C4 | 91.5 (3) | C5–Ru1–C3 | 103.7 (2) |
| C5–Ru1–O1 | 168.7 (2) | C5–Ru1–P2 | 90.0 (2) |
| C5–Ru1–P1 | 89.4 (2) | C4–Ru1–C3 | 89.1 (2) |
| C4–Ru1–O1 | 87.9 (2) | C4–Ru1–P2 | 177.8 (2) |
| C4–Ru1–P1 | 98.0 (2) | C3–Ru1–O1 | 64.9 (2) |
| C3–Ru1–P2 | 89.0 (2) | C3–Ru1–P1 | 165.0 (1) |
| O1–Ru1–P2 | 90.3 (2) | O1–Ru1–P1 | 101.9 (1) |
| P2–Ru1–P1 | 83.64 (8) | | |
| **B. Metal Carbonyls and Phosphines** | | | |
| C21–P1–C11 | 104.2 (2) | C21–P1–C1 | 108.7 (3) |
| C21–P1–Ru1 | 113.6 (2) | C11–P1–C1 | 101.6 (3) |
| C11–P1–Ru1 | 121.7 (2) | C1–P1–Ru1 | 106.0 (2) |
| C31–P2–C41 | 105.9 (3) | C31–P2–C2 | 105.3 (3) |
| C31–P2–Ru1 | 114.1 (2) | C41–P2–C2 | 107.3 (3) |
| C41–P2–Ru1 | 117.3 (2) | C2–P2–Ru1 | 106.1 (2) |
| C2–C1–P1 | 106.9 (4) | C1–C2–P2 | 110.0 (4) |
| O4–C4–Ru1 | 179.0 (6) | O5–C5–Ru1 | 179.3 (6) |
| C12–C11–C16 | 119.8 (5) | C12–C11–P1 | 120.5 (4) |
| C16–C11–P1 | 119.6 (4) | C11–C12–C13 | 119.5 (5) |
| C14–C13–C12 | 120.3 (6) | C13–C14–C15 | 120.8 (5) |
| C14–C15–C16 | 119.2 (6) | C15–C16–C11 | 120.4 (6) |
| C26–C21–C22 | 118.4 (6) | C26–C21–P1 | 124.5 (5) |
| C22–C21–P1 | 116.1 (4) | C23–C22–C21 | 121.2 (6) |
| C22–C23–C24 | 119.3 (7) | C25–C24–C23 | 120.0 (6) |
| C24–C25–C26 | 120.4 (6) | C21–C26–C25 | 120.6 (6) |
| C36–C31–C32 | 119.0 (6) | C36–C31–P2 | 123.2 (4) |
| C32–C31–P2 | 117.8 (5) | C33–C32–C31 | 119.1 (7) |
| C34–C33–C32 | 120.7 (7) | C35–C34–C33 | 119.9 (7) |
| C34–C35–C36 | 120.5 (8) | C31–C36–C35 | 120.7 (7) |
| C46–C41–C42 | 118.9 (6) | C46–C41–P2 | 122.8 (5) |
| C42–C41–P2 | 117.9 (4) | C41–C42–C43 | 121.1 (6) |
| C44–C43–C42 | 118.8 (7) | C45–C44–C43 | 120.2 (7) |
| C44–C45–C46 | 120.7 (6) | C41–C46–C45 | 120.2 (6) |
| **C. [C(O)N(ClC$_6$H$_4$)O]** | | | |
| N1–O1–Ru1 | 91.8 (3) | C3–N1–C51 | 134.4 (4) |
| C3–N1–O1 | 108.6 (4) | C51–N1–O1 | 117.1 (4) |
| O3–C3–N1 | 125.9 (5) | O3–C3–Ru1 | 139.5 (4) |
| N1–C3–Ru1 | 94.7 (3) | C56–C51–N1 | 119.6 (5) |
| C56–C51–C52 | 119.1 (5) | N1–C51–C52 | 121.2 (5) |
| C53–C52–C51 | 119.2 (6) | C54–C53–C52 | 120.2 (5) |
| C53–C54–C55 | 122.1 (6) | C53–C54–CL1 | 119.9 (5) |
| C55–C54–CL1 | 118.0 (5) | C54–C55–C56 | 117.9 (6) |
| C52–C56–C55 | 121.5 (5) | | |

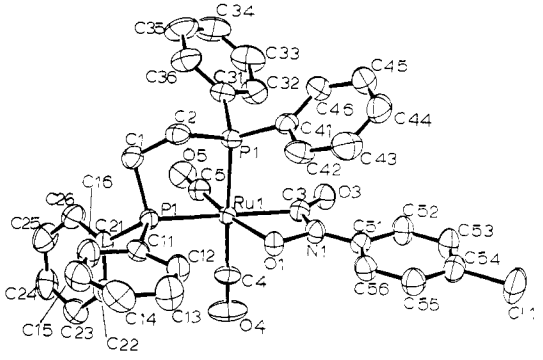


Figure 1. Molecular structure and atom labeling of $Ru(dppe)(CO)_2[C(O)N(Ar)O]$ with thermal ellipsoids shown at the 50% level.

The bond distances and bond angles are listed in Tables II and III. Figure 1 shows the molecular structure of $Ru(dppe)(CO)_2[C(O)N(p\text{-chlorophenyl})O]$.

**Reactions of $Ru(dppe)(CO)_2[C(O)N(o\text{-tolyl})O]$ with $CH_3OH$, $CD_3OD$, $^{13}CH_3OH$, and $H_2O$ under CO Atmosphere.** NMR tubes were attached to 14/20 ground glass joints. Samples were loaded into the NMR tubes in the glovebox. The tubes were capped with Teflon valves and attached to a small, glass manifold constructed for distilling solvent and methanol and adding carbon monoxide to the NMR tubes. Following their addition, the reagents were cooled with liquid $N_2$, and the tubes were sealed. A typical reaction would utilize 20 mg (0.025 mmol) of $Ru(dppe)(CO)_2[C(O)N(o\text{-tolyl})O]$. The sample itself was left under full vacuum for 2.5 h to remove residual solvent of crystallization. $C_6D_6$ (0.6 mL), methanol ($CH_3OH$, $CD_3OD$, or $^{13}CH_3OH$; 0.25 mmol), and CO (≈2 atm) were distilled to the NMR tube using liquid $N_2$.

During ambient temperature reactions, constant mixing of the mixture was facilitated by slow rotation of the NMR tube using a variable-speed overhead stirring apparatus set at 60 rpm. Reactions heated to elevated temperatures were heated in a constant temperature bath without stirring.

**Attempted $^{13}CO$ Labeling of $Ru(dppe)(CO)_2[C(O)N(o\text{-tolyl})O]$ and $Ru(dppe)(CO)_3$.** A glass vacuum apparatus was constructed with three 14/20 ground glass joints and 0.5 in. glass tubing. A sealed glass bulb containing 250 mL of gaseous $^{13}CO$ and a stainless steel breaker was attached directly to the apparatus. A 500-mL storage bulb equipped with a high-vacuum Teflon valve was attached to one joint, and an 80-mL thick-walled glass reaction vessel equipped with a Teflon valve and containing a magnetic stir bar and $Ru(dppe)(CO)_3$ (55 mg, 0.056 mmol) was connected to the other. The vacuum apparatus was then connected to a Schlenk line and evacuated for 2 h. All glass on the apparatus was thoroughly heated with a heat gun to help remove traces of water. Methylene chloride (2.5 mL, degassed and dried over $P_2O_5$) was distilled under vacuum via the Schlenk line to the vessel containing $Ru(dppe)(CO)_3$. The system was isolated from the Schlenk line, and the $^{13}CO$ was released and condensed into the reaction vessel using liquid $N_2$. The reaction vessel was sealed and allowed to warm to room temperature. After the solution was stirred for 3 days at 25 °C, the $^{13}CO$ was transferred to the 500-mL storage vessel, after which the system was opened under a $N_2$ atmosphere. The above procedure was followed for the attempted enrichment of $Ru(dppe)(CO)_2[C(O)N(o\text{-tolyl})O]$ with $^{13}CO$. In neither case was $^{13}CO$ found to exchange with the complexed CO groups.

**Preparation of $Ru(dppe)(CO)_2Cl_2$.** Inside a glovebox a 6 in. test tube was loaded with $Ru(dppe)(CO)_2[C(O)N(o\text{-tolyl})O]$ (100 mg, 0.142 mmol) and sealed with a septum. The tube was removed from the glovebox and 8.0 mL of *o*-xylene was added to the solid via syringe. To this mixture was added 150 μL of a 1.0 M HCl diethyl ether solution. After 3 h the pale yellow microcrystalline solid that formed was filtered on a Schlenk frit, washed with 2 portions of dry hexane (2 mL each), and dried in vacuo to yield 48 mg of $Ru(dppe)(CO)_2Cl_2$ (53% yield). $^1H$ NMR (ppm, $CD_2Cl_2$): 2.6 (m, $CH_2$), 3.1 (m, $CH_2$). $^{31}P$ NMR (ppm, $CD_2Cl_2$): 33.1 (d, $J_{PP}$ = 16 Hz), 56.9 (d, $J_{PP}$ = 16 Hz). $^{13}C$ NMR (ppm, $CD_2Cl_2$): 24.02 (dd, $J_{CP1}$ = 10.7 Hz, $J_{CP2}$ = 31.7 Hz, $CH_2$), 27.20 (dd, $J_{CP2}$ = 10.7 Hz, $J_{CP1}$ = 33.9 Hz, $CH_2$), 189.4 (dd, $J_{CP1}$ = 10.7 Hz, $J_{CP2}$ = 118 Hz, CO), 192.9 (dd, $J_{CP2}$ = 10.7 Hz, $J_{CP1}$ = 13.6 Hz, CO). Mass spectrum ($Ru^{102}$) P (*m/e*): 624. IR ($cm^{-1}$, $CH_2Cl_2$): 2077 (s) and 2007 (s). Anal. Calcd for $Ru(dppe)(CO)_2Cl_2$: C, 53.68; H, 3.88; Cl, 11.32; P, 9.89. Found: C, 53.76; H, 4.04; Cl, 11.51; P, 9.67.

(47) Cromer, D. T.; Ibers, J. A. In Kynoch Press: Birmingham, England, 1974; Vol. IV, Table 2.2C.

**Quantitation of $CO_2$ Evolved during Formation of $Ru(dppe)(CO)_2Cl_2$.** In the glovebox a 5 mm × 7 in. NMR tube was loaded with $Ru(dppe)(CO)_2[C(O)N(o\text{-tolyl})O]$ (10 mg, 0.0142 mmol) and $C_6D_6$ (0.6 mL). The tube was sealed with a septum and removed from the drybox. HCl (56.9 μL, 1.0 M) in diethyl ether (4-fold excess) was injected through the septum. After 20 min $^{31}P$ and $^1H$ spectroscopy revealed 90% conversion to $Ru(dppe)(CO)_2Cl_2$ by integration. Analysis of the headspace of the NMR tube by gas chromatography established that 14% of the 1.9-mL headspace was $CO_2$ at STP. This corresponded to a 91% yield of $CO_2$.

**Synthesis and Spectroscopy of $Ru(dppe)(CO)_2[C(O)OMe]_2$.** A 50-mL stainless steel autoclave containing $Ru(dppe)(CO)_3$ (461 mg, 0.791 mmol) was purged three times with CO. *o*-Nitrotoluene (100 μL, 2.97 mmol) was dissolved in 15 mL of degassed toluene and injected into the autoclave via an exhaust valve. After 5 min 3 mL of methanol was injected in the same manner and the bomb was pressurized with CO (100 psig) and placed in a block heated to 60 °C. After 2 h the reactor was cooled, the pressure was released, and the solution was transferred to a 2-necked 100-mL round-bottomed flask. Solvent was removed in vacuo. The resulting red oil was washed 3 times with 10-mL portions of diethyl ether and evacuated again yielding 285 mg of light brown solid (yield 53%). $^1H$ NMR (ppm, $C_6D_6$): 2.22 (m, $CH_2$), 2.90 (m, $CH_2$), 3.03 (s, $OCH_3$), 3.76 (s, $OCH_3$), 6.99 (m, Ar H), 7.44 (m, Ar H), 7.76 (m, Ar H), 8.02 (m, Ar H). $^{31}P$ NMR (ppm, $C_6D_6$): 46.4 (d, $J_{PP}$ = 10.2 Hz), 51.6 (d, $J_{PP}$ = 10.3 Hz). $^{13}C$ NMR (ppm, $C_6D_6$): 27.0 (dd, $J_{CP1}$ = 12.9 Hz, $J_{CP2}$ = 25.1 Hz, $CH_2$), 48.94 (s, $CH_3$), 50.17 (s, $CH_3$), 195.4 (dd, $J_{CP1}$ = 12.11 Hz, $J_{CP2}$ = 89.5 Hz, CO), 197.8 (dd, $J_{CP1}$ = 9.11 Hz, $J_{CP2}$ = 89.3 Hz, CO), 197.77 ($J_{CP1}$ = 10.58 Hz, $J_{CP2}$ = 6.4 Hz, CO), 199.64 (t, $J_{CP1,CP2}$ = 12.5 Hz, CO). Mass spectrum ($Ru^{102}$) P (*m/e*): 678. IR ($cm^{-1}$, $CH_2Cl_2$): 2048 (s), 1998 (s), 1612 (w). IR ($cm^{-1}$, toluene): 2051 (s), 1999 (s). Anal. Calcd for $Ru(dppe)(CO)_2[C(O)OMe]_2$: C, 57.05; H, 4.50; P, 9.19. Found: C, 56.86; H, 4.68; P, 9.39.

**Thermolysis of $Ru(dppe)(CO)_2[C(O)OMe]_2$.** A sample of $Ru(dppe)(CO)_2[C(O)OMe]_2$ (15 mg, 0.022 mmol) was placed in a NMR tube which was attached to the vacuum line with a ground glass joint. Benzene-$d_6$ (0.6 mL) was distilled into the tube under vacuum, and the tube was sealed and cut from the line using a torch. $^1H$ NMR spectra were collected before and after the tube was heated to 80 °C for 5 h.

**Kinetic Studies.** The reactor system consisted of a 50-mL, overhead-stirred, high-pressure Parr autoclave equipped with a dip tube for removing reaction samples. The autoclave was stored in an oven before each use and was transferred into the glovebox (while still hot) to be loaded with *p*-nitrotoluene (650 mg, 4.74 mmol), naphthalene (70 mg, 0.55 mmol), $Ru(dppe)(CO)_3$ (71 mg, 0.122 mmol) and 20 mL of a 5:1 stock *o*-xylene–methanol solvent. The autoclave was sealed, removed from the glovebox, and connected to a purged stainless steel CO high-pressure line. After purging the reactor with three volumes (13 atm of CO each), the reactor was pressurized to the desired reaction pressure of CO, and all its valves were sealed. The autoclave was placed in an aluminum block that was preheated to the desired reaction temperature. The first sample was collected within 3 min of placing the bomb in the heated block. The reaction was stirred at 80 rpm throughout the catalysis. The temperature of the reactor equilibrated after 15 min, during which time a pressure rise was noted. Samples were collected under a nitrogen atmosphere by inserting the exit from the diptube through a septum capping a nitrogen-filled 10-mL vial that was cooled to approximately −50 °C to minimize loss of methanol during the sampling procedure.

Two injections (0.2 μL) were made for each sample, and the integrated areas of the respective compounds were averaged before calculating concentrations from standard calibration curves. Naphthalene was used as the internal standard.

The procedure followed during the four catalytic reactions spiked with water was identical to the above procedure except that the various amounts of water were introduced by rapidly opening the autoclave and injecting water into the autoclave via microliter syringe prior to purging the reactor with CO (13 atm of CO each).

**High-Pressure FTIR Spectroscopy.** After setup and tuning of the optical bench and cell, 6 mL of solvent (5:1 *o*-xylene–MeOH) was injected to the autoclave via an exhaust port equipped with a septum. The reactor was purged three times with CO (12–15 atmospheres) and then pressurized to a constant 60 atm of CO. Background spectra were collected after the reactor equilibrated under each of the following conditions: 155 °C (78 atm), 22 °C (60 atm), and 22 °C (1 atm). A 2.2-mL solution (5:1 *o*-xylene–MeOH) of $Ru(dppe)(CO)_3$ (118 mg, 0.202 mmol) was injected via the exhaust port under a CO atm. This was followed by a 1.5-mL aliquot of solvent to rinse the lines. *p*-Nitrotoluene (189 mg, 1.38 mmol) dissolved in 2.0 mL of solvent was injected via the same exhaust port followed by a rinse with 1.0 mL of solvent. This brought the total solvent volume to 12.3 mL. The total volume of

the reactor was 50 mL. The reactor was pressurized to 60 atm and allowed to equilibrate for 2.5 h. The reactor was equilibrated at 155 °C approximately 25 min. Infrared spectra were acquired during this procedure and then approximately every half hour until the catalysis was complete (8 h). Typically, 60 scans were collected at a resolution of 2 $cm^{-1}$ requiring 55 s per spectrum.

## Results

We will begin with a description of the characterization of the complexes isolated during the course of this research. Following this summary an outline will be presented of the spectroscopic studies monitoring the formation and reactivity of these complexes. The last two sections will describe the kinetics and in situ FTIR spectroscopy of the catalysis.

**Synthesis and Characterization of Ru(dppe)(CO)$_2$[C(O)N(Ar)O] (Where Ar = *o*-Tolyl (IIa), *p*-Chlorophenyl (IIb), and 2,5-Dimethylphenyl (IIc)).** Formation of IIa, IIb, and IIc occurs under identical conditions for each compound. Equation 3 illustrates the reaction that leads to the essentially quantitative preparation of Ru(dppe)(CO)$_2$[C(O)N(Ar)O] directly from the nitrosoaromatic substrate.

$$Ru(dppe)(CO)_3 + ArNO \rightarrow Ru(dppe)(CO)_2[C(O)N(Ar)O] \quad (3)$$

Mass spectral and elemental analytical data of the crystalline product established that neither CO nor $CO_2$ were evolved. The infrared spectrum of IIa in the $\nu_{CO}$ region exhibited two bands at 2047 and 1972 $cm^{-1}$, which were consistent with the energies of known neutral $Ru^{2+}$ octahedral dicarbonyl complexes.[48] An absorption at 1611 $cm^{-1}$ was attributed to an acyl-like CO. Proton NMR spectroscopy of the *o*-tolyl derivative IIa corroborated the 1:1 stoichiometry between the metal-bound phosphine and the *o*-tolylnitrosobenzene. The broad multiplets at 2.48 and 2.83 ppm due to the ethylene unit of the phosphine ligand and the two distinct resonances seen in the $^{31}P$ NMR spectrum (46.7, 47.1 ppm) established that the two ends of the diphosphine ligand were inequivalent. The $^{13}C$ NMR spectrum of the carbonyl region exhibited three sets of resonances. Two resonances, one at 183.6 ppm (dd, $J_{CP1}$ = 11.2 Hz, $J_{CP2}$ = 82.0 Hz) and the other at 196.6 ppm (dd, $J_{CP1}$ = 7.39 Hz, $J_{CP2}$ = 97.4 Hz), exhibited coupling that suggested a geometry in which the carbons were cis to one phosphorus atom and trans to the other. The resonance at 196.9 ppm (dd, $J_{CP1}$ = 5.44 Hz, $J_{CP2}$ = 13.3 Hz) exhibited coupling consistent with a geometric arrangement in which the carbon was cis to both phosphorus atoms.

These data suggested the structure was one of the two isomers II′ or II″. X-ray structural analysis of the *p*-chlorophenyl complex (Figure 1) definitively established II″ as the correct structure for

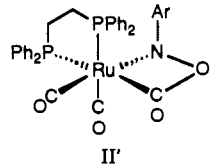


II′

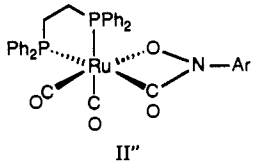


II″

Ru(dppe)(CO)$_2$[C(O)N(Ar)O]. The $^{15}N$ and $^{31}P$ NMR spectra of the isotopically labeled derivative of IIa showed coupling of the nitrogen to one of the phosphorus atoms. The characteristically variable $^{15}N$ $^{13}C$ coupling (+10 to −30 Hz) was not observed in the $^{13}C$ NMR spectrum.[49]

**Structural Analysis of Ru(dppe)(CO)$_2$[C(O)N(ClC$_6$H$_4$)O].** The structure consists of well-separated, slightly-distorted octahedral complexes of $Ru^{2+}$. The Ru(dppe)(CO)$_2$ portion of the structure exhibits typical values for the bond distances and angles. The bite angle for the diphosphine ligand is 83.64 (8)°. There is a significant difference in the length of the Ru–C bond distances of the two carbonyl ligands (Ru–C4 = 1.913 (6) Å and Ru–C5 = 1.855 (6) Å), which is probably due to the difference in the ligand located in the trans position. Trans to C4 is P2, while the ligand trans to C5 is the weakly ligated O1.

The interesting aspects of this structure surround the novel chelating ligand, ClC$_6$H$_4$N(O)CO. To the best of our knowledge the uncomplexed neutral molecule, a *N*-oxoisocyanate, is unknown. The four-membered ring (Ru–O1–N1–C3) is planar and both C51 and O3 lie in that plane. The planar geometry around the nitrogen and the slightly shortened N1–C51 and N1–C3 bond distances of 1.388 (7) and 1.353 (7) Å, respectively, are similar to those of amide structures.[50] The length of N1–O1 (1.414 (5) Å) was longer than those found in amine oxides[50] and that reported in a metal-complexed hydroxamate.[51] It was similar to the N–O bond length observed in various oximes.[50] The Ru–C3 distance of 2.081 (5) Å is typical for $sp^2$-hybridized carbons bound to ruthenium. The Ru–O1 distance of 2.104 (5) Å is long, indicating a relatively weak interaction.

**Synthesis and Characterization of Ru(dppe)(CO)$_2$[C(O)OMe]$_2$.** A high-yield preparation was carried out by reacting I with a 3-fold excess of *o*-nitrotoluene in the presence of methanol and CO. After the solvent was removed under vacuum, the compound was washed with diethyl ether to remove toluidine and excess nitroaromatic. Mass spectral studies established a formula of Ru(dppe)(CO)$_4$(OMe)$_2$ based on the parent ion of 678. The IR spectrum displayed absorptions at 2048, 1998, and 1612 $cm^{-1}$ in the $\nu_{CO}$ region, the lowest energy absorption being characteristic of the methoxycarbonyl ligand.[52] The $^1H$ NMR spectrum exhibited two singlets within the methanolato region (3.03, 3.76 ppm), two broad multiplets at 2.2 and 2.9 ppm resulting from the ethylene unit on the phosphine ligand, and resonances due to the phenyl groups of the ligand. No evidence was found for the presence of an *N*-aryl group. The $^{31}P$ NMR spectrum (d, 45.4 ppm; d, 51.6 ppm) was consistent with an asymmetric compound with the two phosphorus atoms coupled to each other. The $^{13}C$ NMR spectrum of the metal carbonyl region exhibited four resonances. Two of the carbons exhibited coupling, indicating that they were cis to both phosphorus atoms [197.8 ppm ($J_{CP1}$ = 10.58 Hz, $J_{CP2}$ = 6.4 Hz), 199.6 ppm (t, $J_{CP1,CP2}$ = 12.5 Hz)]. The other two carbons were cis to one phosphorus and trans to the other [195.4 ppm (dd, $J_{CP1}$ = 12.11 Hz, $J_{CP2}$ = 89.5 Hz), 197.8 ppm (dd, $J_{CP1}$ = 9.11 Hz, $J_{CP2}$ = 89.3 Hz)]. Structure III is consistent with all the above data.

A lesser amount (20%) of a symmetric isomer (III′ or III″) was present in all solutions of III. The chemical shift for the methyl group in the $^1H$ NMR spectrum was 3.69 ppm, and the resonance at 42.9 ppm in the $^{31}P$ NMR spectrum was also assigned to this isomer.

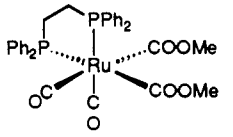


III

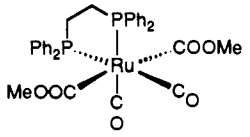


III′

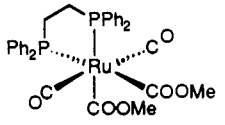


III″

**Characterization of Ru(dppe)(CO)$_2$(OMe)$_2$ and Ru(dppe)(CO)$_2$Cl$_2$.** The first observable compound in the $^1H$ and $^{31}P$ NMR spectra during studies of the reaction of methanol with II was proposed to be Ru(dppe)(CO)$_2$(OMe)$_2$. The two methoxide signals of identical relative intensity at 3.46 and 3.57 ppm in the proton spectrum (Figure 2) corresponded to two new signals in the $^{31}P$ NMR spectrum (Figure 3). The NAr group, originally present in II, was converted to aniline. The formulation of IV

(48) Seddon, E. A.; Seddon, K. R. *The Chemistry of Ruthenium*; Elsevier: Amsterdam, 1984.
(49) Mason, J. *Multinuclear NMR*; Plenum: New York, 1987.
(50) Allen, F. H.; Kennard, O.; Watson, D. G.; Brammer, L.; Orpen, A. G.; Taylor, R. *J. Chem. Soc., Perkin Trans. 2* **1987**, S1–S19.
(51) Lindner, H. J.; Göttlicher, S. *Acta Crystallogr.* **1969**, *B25*, 832.
(52) Ford, P. C.; Rokicki, A. *Adv. Organomet. Chem.* **1988**, *28*, 139.

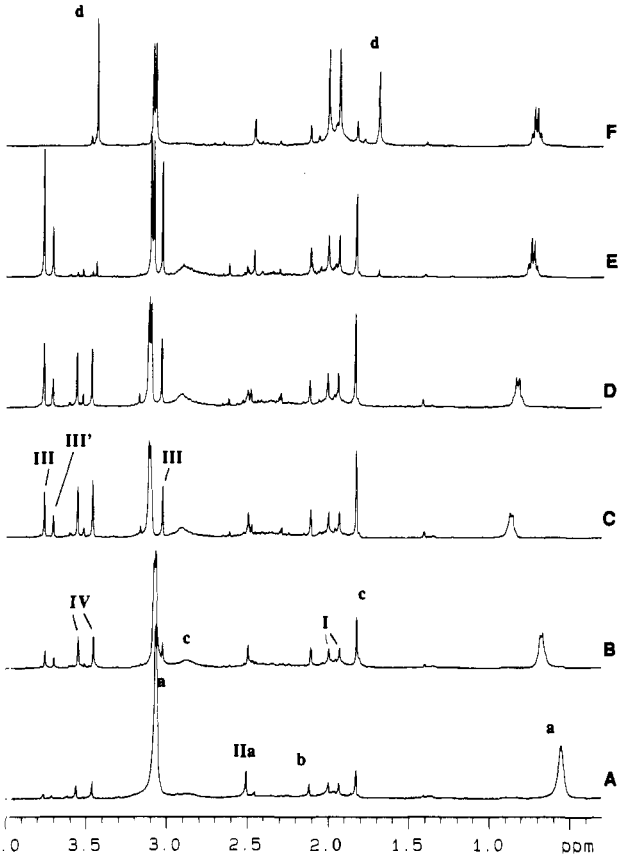


**Figure 2.** Proton NMR spectral series for the reaction of IIa with a 10-fold excess of methanol in benzene-$d_6$ under 2.5 atm of CO: (A) 5.1 h, (B) 15.5 h, (C) 29.7 h, (D) 37.5 h, (E) 74.0 h, (F) After heating at 103 °C for 10 h [a, methanol; b, toluene; c, *o*-toluidine; d, methyl *N*-*o*-tolylcarbamate].

was based in part on its observed conversion into III under a CO atmosphere.

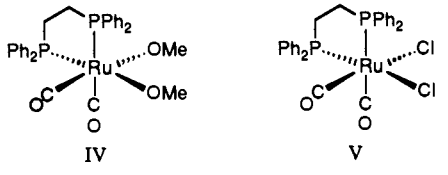


Compound II was found to react with other Brönsted acids. Anhydrous HCl rapidly converts II into the dichloride, V, according to eq 4. Although the formula of V was previously reported, no NMR data were available.[53]

$$Ru(dppe)(CO)_2[C(O)N(Ar)O] + 2HCl \rightarrow CO_2 + ArNH_2 + Ru(dppe)(CO)_2Cl_2 \quad (4)$$

The formulation and structure of V was established using NMR and IR spectroscopy and mass spectral data. The mass spectrum of the compound gave a parent ion of 624 consistent with a formula of $Ru(dppe)(CO)_2Cl_2$. The $^1H$ NMR spectrum was devoid of resonances aside from the phenyl groups and ethylene backbone of the phosphine ligand. The $^{31}P$ NMR spectrum showed only two resonances (33.1 and 56.9 ppm), each with the usual phosphorus–phosphorus coupling of dppe. In the carbonyl region of the $^{13}C$ NMR spectrum two resonances were observed. One exhibited a cis arrangement to both of the phosphorus atoms [192.9 ppm (dd, $J_{CP2}$ = 10.7 Hz, $J_{CP1}$ = 13.6 Hz)], while the other displayed one cis and one trans coupling constant to the chelating phosphorus atoms [189.4 ppm (dd, $J_{CP1}$ = 10.7 Hz, $J_{CP2}$ = 118 Hz)]. The $\nu_{CO}$ for $Ru(dppe)(CO)_2Cl_2$ were located at 2077 and 2007 $cm^{-1}$.

(53) Bruce, M. I.; Stone, F. G. A. *J. Chem. Soc. A* **1967**, 1238.

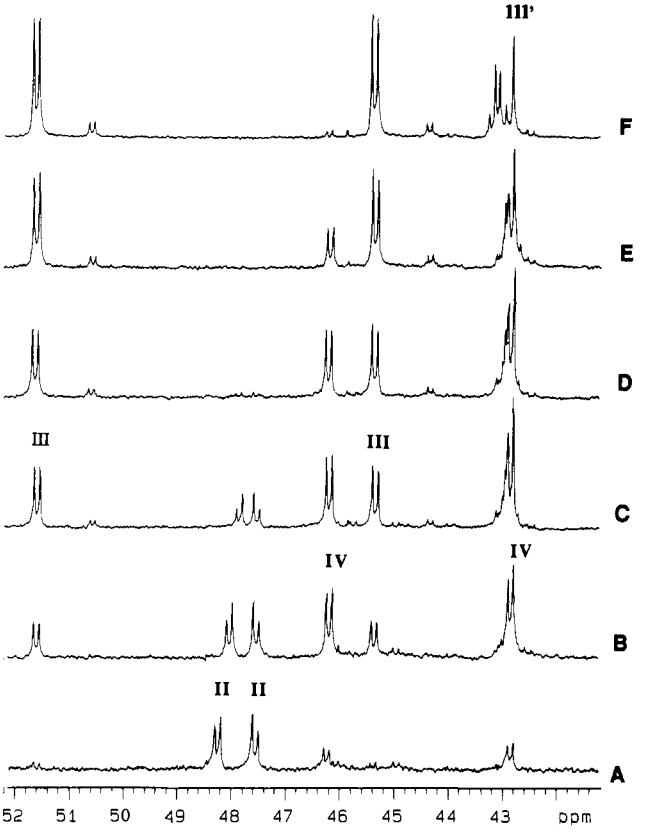


**Figure 3.** Phosphorus-31 NMR series for the reaction of IIa with a 10-fold excess of methanol in benzene-$d_6$ under 2.5 atm of CO: (A) 5.1 h, (B) 15.5 h, (C) 29.7 h, (D) 37.5 h, (E) 60.5 h, (F) 74.0 h. The doublet of doublets at 43.0 ppm is due to an unidentified species. The resonance for I appears as a singlet at 73.3 ppm.

**Reaction of Ru(dppe)(CO)$_3$ with *p*-Chloronitrobenzene and *p*-Chloronitrosobenzene.** During the reaction of $ClC_6H_4NO_2$ with $Ru(dppe)(CO)_3$ 1 equiv of $CO_2$ was produced and 1 equiv of CO was consumed rapidly. Loss of the second equivalent of $CO_2$ required several hours at room temperature. The rate of loss of the second equivalent of $CO_2$ was identical to the rate of loss of $CO_2$ observed when *p*-chloronitrosobenzene was mixed with $Ru(dppe)(CO)_3$. The loss of the second $CO_2$ corresponds to the reaction of $Ru(dppe)(CO)_2[C(O)N(p\text{-chlorophenyl})O]$, IIb, with methanol discussed in the following section. Infrared spectral changes observed during this reaction were described in our earlier publication. Relatively rapid formation of **IIb** was followed by a slower transformation to a solution exhibiting broad absorptions at approximately 2000 and 2055 $cm^{-1}$. Correlation of these infrared spectral results with the NMR spectral studies described below allows us to assign these bands to a mixture of the bis(methanolato) and bis(methoxycarbonyl) complexes. We had proposed in the earlier studies that these peaks were attributable to an amido intermediate.

**Reaction of Ru(dppe)(CO)$_2$[C(O)N(*o*-tolyl)O] with Methanol and HCl.** The reactivity of IIa with methanol was studied under a variety of conditions. In a sealed NMR tube at 70 °C for 10 h under a CO atmosphere IIa was converted into $Ru(dppe)(CO)_3$ in 35% yield and a new organometallic complex, $Ru(dppe)(CO)_2[C(O)OMe]_2$, in 60% yield. A nearly quantitative yield (95%) of *o*-toluidine ($ArNH_2$) was observed. About 5% of the metal species exists as an as yet unidentified species ($^{31}P$ NMR: d, 43.1 ppm; d, 43.3 ppm). Only a trace of carbamate was formed.

The results obtained from the reaction of $Ru(dppe)(CO)_2[C(O)N(o\text{-tolyl})O]$ with $CD_3OD$ under CO were identical with those of the reaction above. Methanol-$d_4$ reacts with $Ru(dppe)(CO)_2[C(O)N(Ar)O]$ under mild conditions to form a 55% yield of $Ru(dppe)(CO)_2[C(O)OCD_3]_2$, 40% yield of $Ru(dppe)(CO)_3$, and 95% of *o*-toluidine-$d_2$. Because the $^1H$ signals were absent, this experiment shows conclusively that the methyl peaks from

**Table IV.** Catalytic Runs Spiked with Water[a]

| $p_{CO}$ (atm) | $[H_2O]_i$[b] | [Ru][b] | $[NO_2]_i$[b] | conversion[c] | selectivity[c] | $k_{a(obs)}$[d] |
|---|---|---|---|---|---|---|
| 74.5 | 0.0 | 4.9 | 248 | 95.9 | 86.0 | 0.797 |
| 82.6 | 32 | 3.2 | 152 | 94.3 | 64.7 | 9.33 |
| 82.6 | 60 | 2.8 | 114 | 80.1 | 16.4 | 51.3 |
| 82.6 | 111 | 3.3 | 126 | 79.4 | 8.8 | 71.0 |

[a] All reactions performed at 145 °C and 5.0 M methanol. [b] Concentration in mM based on the measured material placed in the reactor before heating. [c] Conversion is defined as ([final carbamate] + [final *p*-toluidine])/[initial nitroaromatic] × 100%. Selectivity for carbamate over aniline defined as [final carbamate]/([final *p*-toluidine] + [final carbamate]) × 100%. [d] $k_{a(obs)}$ = ([slope of the toluidine formation curve) × $p_{CO}$]/[Ru]).

$Ru(dppe)(CO)_2[C(O)OCD_3]_2$ were derived from methanol, as were the amine protons.

The results of the room temperature reaction of Ru(dppe)-$(CO)_2[C(O)N(o\text{-tolyl})O]$ with methanol under CO were monitored by $^1H$ and $^{31}P$ NMR spectroscopy and are shown in Figures 2 and 3, respectively. After 75 h, $^1H$ NMR spectroscopy established the formation of *o*-toluidine, $Ru(dppe)(CO)_2[C(O)OMe]_2$ (III), and $Ru(dppe)(CO)_3$ (I) in yields similar to the experiment conducted at 70 °C. Although the same endpoint was reached, a new species, IV, was observed as IIa disappeared and prior to formation of III.

The singlet at 2.51 ppm (Figure 2) corresponds to the *o*-methyl hydrogen atoms on the *N*-aryl moiety of IIa. Under the concentration regime used for these reactions, IIa was only partially soluble in $C_6D_6$ at this temperature. After approximately 34 h, the mixture became homogeneous and by 37 h IIa was consumed. The peak at 2.12 ppm was due to trace toluene originating from the preparation of IIa, and it was used as an internal integration standard for this particular run. Methanol, present in a 10-fold excess, gave a variable signal for the alcoholic proton which has an exchange-dependent chemical shift in the range between 0.53 and 0.75 ppm. Exchange dissipates upon consumption of IIa (see Figure 2, spectrum E).

The species responsible for the peaks at 3.46 and 3.57 ppm ($^1H$) corresponded to an as yet unisolated species believed to be Ru-$(dppe)(CO)_2(OMe)_2$ (IV). This species appeared prior to the formation of III, and it was also observed in the thermolysis of III under a vacuum.

Phosphorus-31 NMR spectra showing the formation and disappearance of III and IV are given in Figure 3. Consistent with the $^1H$ NMR spectra, complete consumption of IV was noted after 75 h.

At room temperature no further change was noted in the spectra for days once IV was consumed. At this point, the reaction of III with *o*-toluidine was initiated by heating the sealed NMR tube to a temperature of 103 °C. After the reaction was heated for 10 h, the $^1H$ and $^{31}P$ NMR spectra showed that the reaction of III with aniline quantitatively produced $Ru(dppe)(CO)_3$ and methyl *N*-*o*-tolylcarbamate.

The importance of the acidic hydrogen of methanol to the above conversion was suggested by studying the analogous reaction using a stronger acid. Upon addition of anhydrous HCl to II at room temperature, immediate formation of $CO_2$, $ArNH_2$, and Ru-$(dppe)(CO)_2Cl_2$ was observed. Water was found to react slowly with II at room temperature to give $ArNH_2$, $Ru(dppe)(CO)_3$, and presumably $CO_2$.

**Kinetic Results.** The catalytic kinetics for $Ru_3(CO)_{12}$ were studied in detail by Grate and co-workers.[11-14] They also performed studies of several related ruthenium carbonyl catalysts, including $Ru(dppe)(CO)_3$, which established a similarity to the kinetics obtained for $Ru_3(CO)_{12}$.[54] For us to relate our stoichiometric and in situ spectroscopic studies to the kinetics in order to propose a mechanism, it was critical to conduct a detailed kinetic analysis of the catalysis using $Ru(dppe)(CO)_3$. The results of this are summarized in this section.

(54) Grate, J. H. Personal communication.

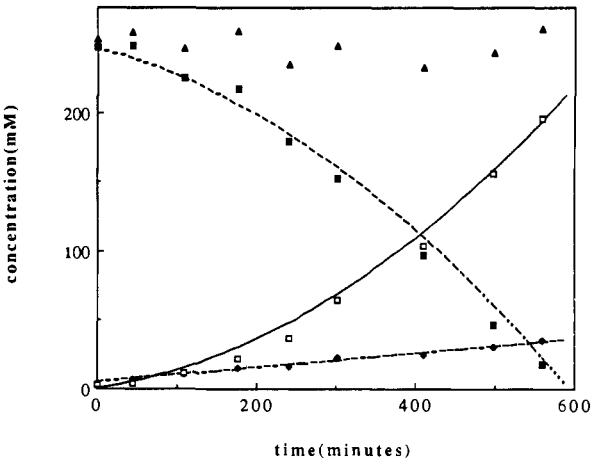


**Figure 4.** Progress of a catalytic reaction conducted in *o*-xylene at 145 °C, $p_{CO}$ = 48 atm with $[Ru(dppe)(CO)_3]$ = 5.2 mM, [*p*-nitrotoluene]$_i$ = 230 mM, and [methanol] = 5.0 M: (■) *p*-nitrotoluene, (●) *p*-toluidine, (□) methyl *N*-*p*-tolylcarbamate, and (▲) mass balance. The lines are the fits from the kinetic model described in the text.

After many kinetic runs of poor reproducibility it was established that trace amounts of water had a considerable impact on the catalysis. When water was added, aniline formation occurred at a much higher rate until the water was consumed. Table IV illustrates the effect that varied amounts of added water had on the outcome of the product distribution and the rate of reaction. These results are in agreement with the observations reported by Grate and co-workers.[11-14] The observation is also consistent with the studies of Pettit and co-workers showing that metal carbonyls catalyze the reduction of nitroaromatics under water-gas shift (CO + $H_2O$) conditions.[55] It is noteworthy that even under completely dry conditions a small amount of aniline ($[ArNH_2]_i$) was observed by the time the first sample was withdrawn for analysis (ca. 3 min after heating was begun). Over all the kinetic runs in which no external aniline or water was added, the ratio $[ArNH_2]_i$/$[Ru(dppe)(CO)_3]$ was equal to 0.9 ± 0.2. This suggests that 1 equiv of aniline is produced in parallel to the relatively rapid conversion of $Ru(dppe)(CO)_3$ into the predominant metal-containing species present during catalysis.

Under dry conditions the first notable aspect of the catalysis is the curvature of the lines showing the disappearance of substrate and the formation of carbamate (Figure 4). The catalytic reaction rate increased as the reaction proceeded. The concentration of aniline, however, increased at a constant rate throughout the catalysis. A scenario that could explain the curvature was that the rate of carbamate formation was dependent on the aniline concentration, as previously concluded by Grate and co-workers.[11-14] In accordance with this hypothesis, adding aniline to the starting catalysis solution increased the rate of the reaction. The curvature complicated the analysis of the effect of reaction parameters on the rate. During our initial studies, we utilized the tangent to the curve when the reaction was approximately 50% complete as an estimate of the rate. After developing the kinetic model described below, all of the kinetic runs were reanalyzed to give the values of $k_{a(obs)}$ and $k_{c(obs)}$ presented in Table V.

The rates of both aniline (Figure 5) and carbamate production displayed a first-order dependence on the concentration of the ruthenium catalyst. Under all conditions studied, the rates were independent of the concentration of the starting nitroaromatic. Variation of the methanol concentration between 5 and 25 M (neat methanol) also had no effect on the catalytic rates. As the methanol concentration was lowered below 5 M, the rate of aniline production dropped while carbamate production remained unchanged. Variation of the CO pressure caused both rates to change. The rates *decreased* as the pressure was increased from 14 to 82 atm. A plot of the rate of aniline production versus $1/p_{CO}$

(55) Cole, T.; Ramage, R.; Cann, K.; Pettit, R. *J. Am. Chem. Soc.* **1980**, *102*, 6182.

**Table V.** Summary of Kinetic Data

| $p_{CO}$ (atm) | temp (°C) | [Ru][a] | $[NH_2]_i$[a,b] | [MeOH][c] | $[NO_2]_i$[a,d] | conversion[e] | selectivity[f] | $k_{a(obs)}$[g] | $k_{c(obs)}$[h] |
|---|---|---|---|---|---|---|---|---|---|
| | | | | Variation of $p_{CO}$ | | | | | |
| 22.4 | 145 | 6.1 | 3.0/4.2 | 5.0 | 240 | 94.6 | 75.5 | 0.741 | 6.7 |
| 32.2 | 145 | 5.6 | 3.0/5.3 | 5.0 | 275 | 91.3 | 83.4 | 0.700 | 5.2 |
| 48.0 | 145 | 5.1 | 2.2/3.8 | 5.0 | 230 | 97.3 | 83.2 | 0.538 | 5.6 |
| 74.5 | 145 | 4.9 | 5.0/4.2 | 5.0 | 248 | 95.5 | 86.0 | 0.797 | 4.1 |
| 103.1 | 145 | 5.4 | 4.5/4.9 | 5.0 | 240 | 97.0 | 83.9 | 0.773 | 4.1 |
| | | | | Variation of *p*-Toluidine Concentration | | | | | |
| 48.0 | 145 | 5.1 | 2.2 | 5.0 | 230 | 97.3 | 83.2 | 0.538 | 5.6 |
| 49.0 | 145 | 5.7 | 20 | 5.0 | 230 | 91.2 | 98.8 | 0.598 | 4.6 |
| 49.0 | 145 | 5.8 | 34 | 5.0 | 238 | 94.1 | 90.2 | 0.632 | 3.8 |
| 47.6 | 145 | 5.7 | 52 | 5.0 | 240 | 93.7 | 92.6 | 0.604 | 2.9 |
| | | | | Variation of Catalyst Concentration | | | | | |
| 48.0 | 145 | 11.2 | 8.0/5.0 | 5.0 | 231 | 96.1 | 88.5 | 0.480 | 5.2 |
| 48.0 | 145 | 5.2 | 2.2/3.8 | 5.0 | 230 | 97.3 | 83.2 | 0.538 | 5.6 |
| 49.0 | 145 | 1.3 | 1.0/1.5 | 5.0 | 234 | 90.0 | 81.6 | 0.573 | 4.0 |
| | | | | Variation of Methanol Concentration | | | | | |
| 50.3 | 145 | 5.1 | 9.3/5.3 | 24.7 | 235 | 93.7 | 83.0 | 0.578 | 5.5 |
| 50.3 | 145 | 5.3 | 3.4/4.4 | 7.4 | 243 | 92.2 | 84.4 | 0.543 | 5.0 |
| 48.0 | 145 | 5.2 | 2.2/3.8 | 5.0 | 230 | 97.3 | 93.2 | 0.537 | 5.6 |
| 48.3 | 145 | 4.9 | 4.6/5.0 | 2.6 | 240 | 98.9 | 90.0 | 0.256 | 5.7 |
| 49.1 | 145 | 5.3 | 4.6/4.5 | 1.2 | 230 | 97.0 | 94.5 | 0.162 | 8.5 |
| | | | | Variation of Reaction Temperature | | | | | |
| 45.4 | 125 | 6.6 | 6.9/5.2 | 5.0 | 246 | 92.4 | 91.4 | 0.045 | 1.6 |
| 47.6 | 135 | 5.1 | 5.1/4.2 | 5.0 | 241 | 95.0 | 89.0 | 0.142 | 2.4 |
| 48.0 | 145 | 5.2 | 2.2/3.8 | 5.0 | 230 | 97.3 | 83.2 | 0.538 | 5.7 |
| 48.3 | 155 | 5.0 | 4.6/5.7 | 5.0 | 241 | 95.0 | 85.0 | 0.618 | 7.5 |

[a] Concentration in mM. [b] The first value gives initial concentration based on the *y* intercept of the aniline concentration curve, the second based on GC integration. [c] Concentration in M. [d] Initial *p*-nitrotoluene concentration based on a calculation from initial weight. [e,f] Conversion and selectivity are defined as specified in Table IV. [g] $k_{a(obs)}$ = [(slope of the aniline formation curve) × $p_{CO}$)]/[Ru]. [h] $k_{c(obs)}$ was derived from the best fit of the data using the kinetic model.

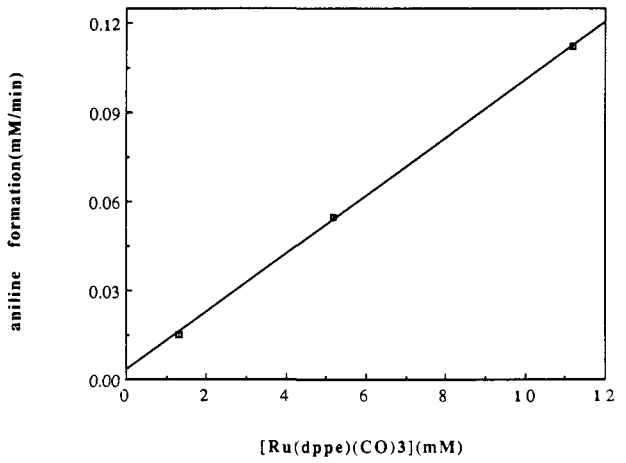


**Figure 5.** Rate of formation of *p*-toluidine vs initial catalyst concentration.

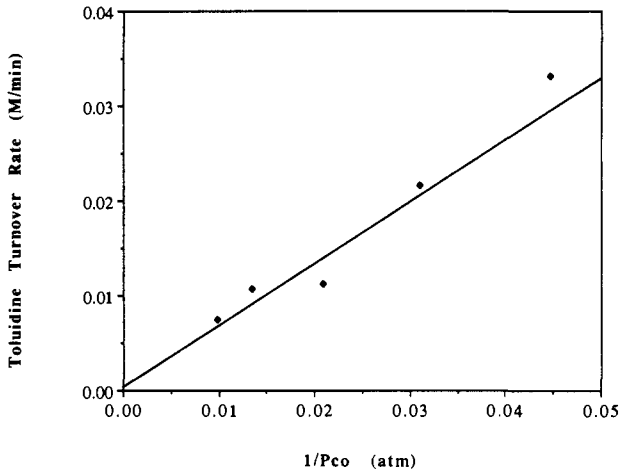


**Figure 6.** Rate of *p*-toluidine formation vs $1/p_{CO}$. The solid line is based on the kinetic model described in the text.

is linear (Figure 6). The decrease in the rate of carbamate production can be explained by its dependence on the rate of aniline production. Adding aniline to the starting reaction solution had no effect on the rate of production of additional aniline. It did, however, increase the rate of carbamate synthesis. The dependence on aniline concentration was first order between 0 and 50 mM of aniline. This range corresponds to 0 to 0.2 equiv of aniline relative to the starting concentration of nitroaromatic.

At initial concentrations of aniline greater than 100 mM significant deviation from the rate law derived below was observed. The mass balance displayed a minimum when the reaction was halfway toward completion. Samples withdrawn from the reactor contained noticable amounts of a white, crystalline solid which was found to be the corresponding *N,N'*-diarylurea. Under the conditions of the reaction the urea eventually undergoes methanolysis to form aniline and carbamate. This is consistent with the observations made by Grate and co-workers.[11-14] Under catalytic conditions, but without the catalyst, methanolysis of *N*-(*o*-tolyl)-*N'*-(*p*-chlorophenyl)urea led to a product distribution of 1:2.2 of methyl *N*-*p*-tolylcarbamate and *p*-chloroaniline to methyl *N*-(*p*-chlorophenyl)carbamate and *p*-toluidine. Most of the reactions were studied under conditions that avoided the formation of observable amounts of urea. One exception to this involved the catalytic production of urea in the absence of any methanol. The results of two experiments, identical in all ways ($T$ = 145 °C, $p_{CO}$ = 45 atm, [Ru(dppe)$(CO)_3$] = 3.8 mM, [*p*-nitrotoluene] = 97 mM, [*p*-toluidine] = 161 mM) except that one included methanol (2.5 M) and the other did not, established that the rate of disappearance of nitroaromatic was slower by a factor of 18 without methanol.

The formation of a mixture of carbamates resulted from conducting the catalytic reaction in the presence of different aryl groups on the aniline and nitroaromatic.[12] In our hands this experiment consisted of adding *p*-chloroaniline (0.190 M) to a catalytic mixture comprised of *p*-nitrotoluene (0.250 M), methanol (5.0 M), and Ru(dppe)$(CO)_3$ (0.004 M). The solvent (*o*-xylene), temperature (145 °C), and pressure (65 atm) were typical. At

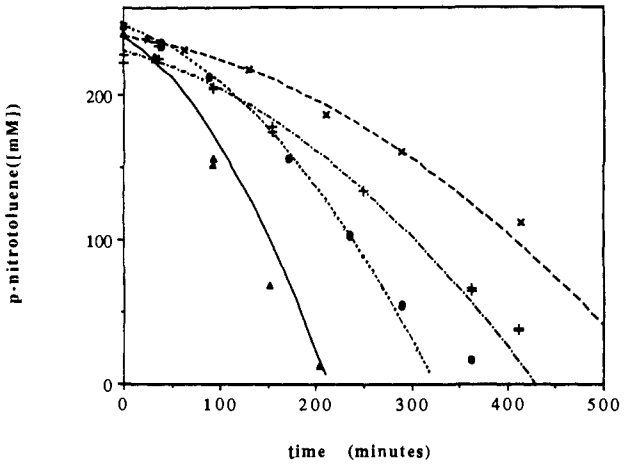


**Figure 7.** Actual vs calculated *p*-nitrotoluene consumption during reactions performed at the following pressures: (△) 22.4 atm, (●) 32.2 atm, (+) 48.0 atm, (×) 103.1 atm.

the end of the catalysis, the mixture consisted of *p*-chloroaniline, *p*-toluidine, methyl *N*-*p*-tolylcarbamate, and methyl *N*-(*p*-chlorophenyl)carbamate. More revealing was the observation that during the first 25% of the reaction, methyl *N*-(*p*-chlorophenyl)carbamate was the major carbamate observed. A control experiment was conducted to determine whether or not significant exchange of the *N*-aryl groups occurred under the conditions of this experiment. An *o*-xylene/methanol (5:1) solution containing *p*-chloroaniline (0.2 M) and methyl *N*-*o*-tolylcarbamate (0.4 M) showed no exchange for 17 h at 145 °C. Taken together, these experiments establish that free amine is consumed in the carbamate-producing step of the catalysis.[12]

The experimentally derived rate expressions for the formation of aniline and carbamate are shown in eqs 5 and 6

$$d[ArNH_2]/dt = k_{a(obs)}[Ru]/p_{CO} \quad (5)$$

$$d[Carb]/dt = k_{c(obs)}[Ru][ArNH_2] \quad (6)$$

where [Ru], [$ArNH_2$], and [Carb] represent the concentrations of the ruthenium catalyst, *p*-toluidine, and methyl *N*-*p*-tolylcarbamate, respectively. The CO pressure in atmospheres is represented by $p_{CO}$, and $k_{a(obs)}$ and $k_{c(obs)}$ are the observed rate constants for the formation of *p*-toluidine and methyl *N*-*p*-tolylcarbamate, respectively. Both $p_{CO}$ and [Ru] are treated as constants. Integration of eq 5 gives

$$[ArNH_2]_t = [ArNH_2]_i + (k_{a(obs)}[Ru]/p_{CO})t \quad (7)$$

where $[ArNH_2]_i$ and $[ArNH_2]_t$ are the initial *p*-toluidine concentration and the concentration of *p*-toluidine at time *t*, respectively. Substitution of this expression into eq 6 and integration yields eq 8.

$$[Carb]t = k_{c(obs)}[Ru][ArNH_2]_i t + \{(k_{c(obs)}k_{a(obs)}[Ru]^2)/2p_{CO}\}t^2 \quad (8)$$

From the mass balance (eq 9), we can obtain an expression that can be used to calculate the concentration of nitroaromatic as a function of time, $[ArNO_2]_t$.

$$[ArNO_2]_t = [ArNO_2]_i - \{[ArNH_2]_t - [ArNH_2]_i\} - [Carb]_t \quad (9)$$

The rate constant for *p*-toluidine formation ($k_{a(obs)}$) was derived from the slope of the plot of [$ArNH_2$] vs time, and the intercept was used as $[ArNH_2]_i$. The rate constant, $k_{c(obs)}$, was determined by fitting curves of the expressions for $[Carb]_t$ and $[ArNO_2]_t$ to the experimental data. An example of such a fit is shown in Figure 4. Figure 7 demonstrates that the model successfully predicts the reaction progress even over a wide range of CO pressures. At 145 °C, the average value of $k_{a(obs)}$ was 0.65 ± 0.10 atm $min^{-1}$ and the average value of $k_{c(obs)}$ was 5.0 ± 0.9 $M^{-1}$ $min^{-1}$. This model gave reasonable fits for all experimental runs even though

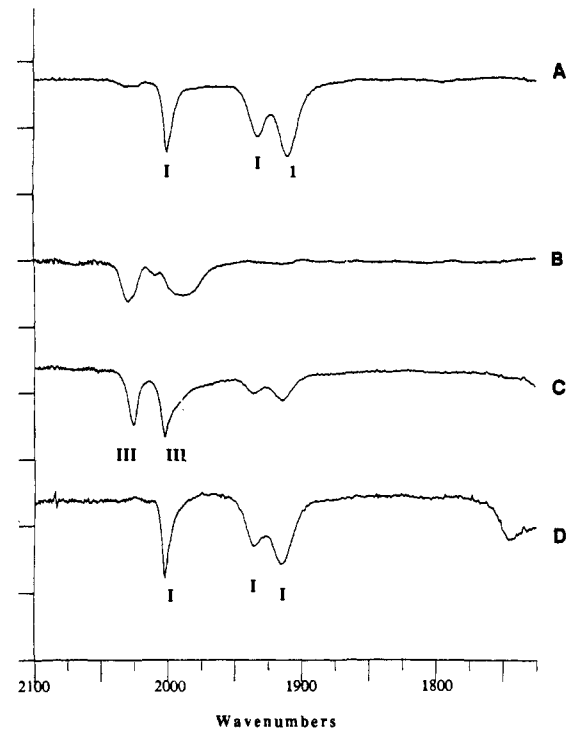


**Figure 8.** In situ high-pressure FTIR spectra of a catalytic reaction: (A) before mixing substrate with catalyst, $T$ = 25 °C, $p_{CO}$ = 1 atm; (B) 100 minutes after mixing catalyst and substrate, $T$ = 25 °C, $p_{CO}$ = 60 atm; (C) 51 min after initial heating and stirring, $T$ = 155 °C, $p_{CO}$ = 66 atm; (D) cooled reaction solution after the catalysis is complete, $T$ = 45 °C, $p_{CO}$ = 1 atm. Conditions: [$Ru(dppe)(CO)_3$] = 16 mM, [*p*-nitrotoluene] = 109 mM, solvent = 5:1 *o*-xylene–methanol. The absorption at 1735 $cm^{-1}$ is due to carbamate. Spectrum B shows a mixture of $Ru^{2+}$ species.

temperature control was limited to ±1 °C. The other difficulty in analyzing kinetic data from high-pressure autoclaves is the definition of the beginning of the reaction. We attempted to minimize the impact of the time required to raise the temperature of the autoclave to the desired value by studying the reaction at temperatures slightly lower than those reported in the original patents (160 °C). This lengthened the overall reaction time and reduced the impact of the reactor equilibration period.

Varying the temperature of the reaction between 125 and 155 °C allowed the determination of the Arrhenius parameters for both the aniline and carbamate producing steps. For aniline formation, $A = 4.3 \pm 0.8 \times 10^{15}$ M/min and $E_a = 31 \pm 6$ kcal/mol, and for carbamate production, $A = 2.6 \pm 0.3 \times 10^{10}$ M/min and $E_a = 19 \pm 3$ kcal/mol.

**Spectroscopy of the Catalytic Solutions.** Figure 8 illustrates infrared spectra collected during the course of a typical catalytic reaction. Spectrum A shows the catalyst before mixing with *p*-nitrotoluene. Interaction of $Ru(dppe)(CO)_3$ and *p*-nitrotoluene for 2.5 h under 87 atm of CO at ambient temperature results in oxidation of the metal center with formation of a mixture of compounds having two broad absorptions in the IR centered at 1980 and 2060 $cm^{-1}$ (spectrum B). These absorptions are similar to that of II, the nitroso adduct formed with the *o*-tolyl species. Upon heating the autoclave to 155 °C, the peaks sharpened into absorptions at 2053 and 2000 $cm^{-1}$ (spectrum C), which are characteristic of those of the bis(methoxycarbonyl) complex III. These remain until the end of the reaction when they are slowly replaced by the absorptions due to the initial complex, $Ru(dppe)(CO)_3$. The absorption at 1735 $cm^{-1}$ is due to the carbamate.

Samples of the catalysis solutions were also studied using $^{31}P$ NMR spectroscopy (Figure 9). Rapid quenching of the samples was accomplished by withdrawing them under $N_2$ into a vial cooled to approximately −50 °C. Resonances located at 42.9, 45.4, and 51.6 ppm accounted for greater than 80% of the total signal intensity and are attributed to compound III.

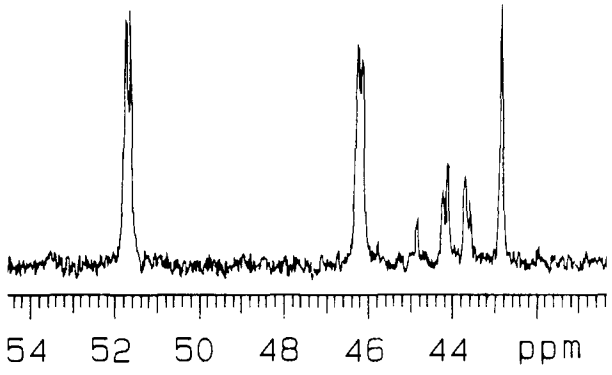


**Figure 9.** Phosphorus-31 NMR spectrum of a typical catalytic reaction. The sample was removed from the autoclave via the dip tube 55 min into the run. The spectrum was obtained directly from the catalytic solution. Conditions: $p_{CO}$ = 48 atm, $T$ = 145 °C, [Ru] = 11.2 mM, [*p*-nitrotoluene] = 231 mM.

**Scheme I.** Overall Catalytic Cycle

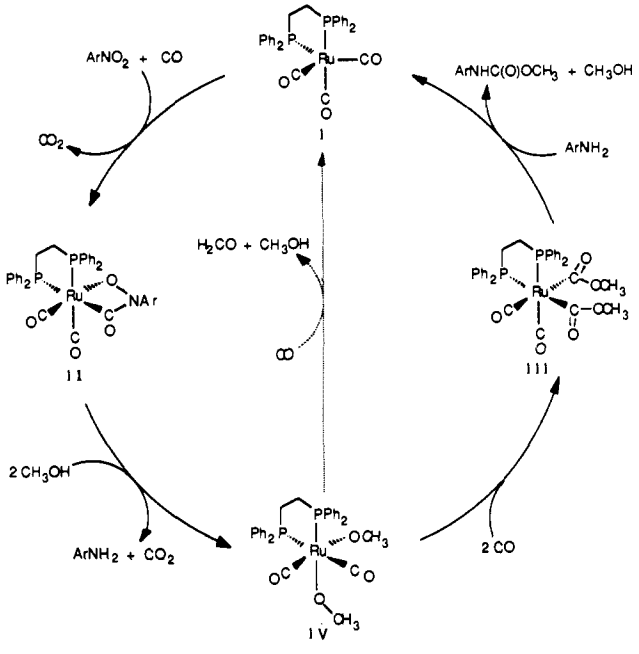


## Discussion

The study of stoichiometric reactions has provided a framework shown in Scheme I for discussing the possible mechanisms of the catalytic process. The discussion will follow the process through three phases: the first deoxygenation, the second deoxygenation and the formation of aniline, and formation of carbamate. The last sections will relate the kinetic and in situ spectroscopic studies to the stoichiometric reactions.

**Phase 1: The First Deoxygenation of the Nitroaromatic.** Immediately following the mixing of the substrate, *p*-chloronitrobenzene, with the catalyst, $Ru(dppe)(CO)_3$, in the *o*-xylene/MeOH solvent mixture under CO, a reaction occurs. One equivalent of $CO_2$ is lost, and 1 equiv of CO is absorbed. The infrared spectra data indicate the formation of a six-coordinate, $Ru^{2+}$ complex, $Ru(dppe)(CO)_2[C(O)N(Ar)O]$; however, no intermediates are observed. The same product could be formed quantitatively by reacting the corresponding nitrosoarene with $Ru(dppe)(CO)_3$. The starting ruthenium complex is a robust, 18-electron, coordinatively-saturated species which does not readily lose its ligands under such mild conditions. For example, ligand exchange with an atmosphere of $^{13}CO$ would provide some measure of the ability of $Ru(dppe)(CO)_3$ to form an unsaturated site by CO dissociation or formation of a dangling phosphine ligand. No such exchange was observed after 3 days of stirring a toluene solution of $Ru(dppe)(CO)_3$ under $^{13}CO$ at room temperature.

The above argument does not preclude the possibility that the nitroaromatic could act as a nucleophile in a bimolecular type of reaction. This possibility can be dismissed on the basis of the known nonnucleophilic behavior of nitroaromatics. One measure of this invokes the relationship between nucleophilicity toward metals vs protons. The $pK_a$ of the conjugate acid of nitroaromatics ($ArNO_2H^+$) is −12, the most negative of any organic functional group.[56] In addition, there are no crystallographically characterized examples of nitroarene complexes to transition metals. The danger of such an argument is that successful synthetic routes to the complexes have not been developed. This can be ruled out on the basis of the successful characterization of $[Zn(PhNO_2)_n(OTeF_5)_2]$ ($n$ = 2, 3) by Strauss and co-workers.[57] Only with the remarkably nonnucleophilic teflate ion ($F_5TeO^-$) could this interaction be observed. Haloalkanes were found to be stronger ligands than the nitroaromatics. Crabtree and co-workers reported that the electrophilic iridium complex, $Ir^{3+}$, could be stabilized by nitrobenzene.[58] Once again a parallel between haloalkane complexes and nitroarene complexes could be drawn. These studies clearly demonstrate the very weak nucleophilic behavior of nitroaromatics.

An alternative first step in the mechanism to forming a direct bond between the metal and the nitroaromatic involves a single electron transfer from the metal to the nitroaromatic. An important precedent for this mechanism exists in the study by Kochi and co-workers of eq 10.[59] The rate-determining step was a single electron transfer between $PhNO_2$ and $Ni(PPh_3)_3$.

$$Ni(PPh_3)_4 + PhNO_2 \rightarrow Ni(PPh_3)_2(\eta^2\text{-PhNO}) + OPPh_3 + PPh_3 \quad (10)$$

In this ruthenium system, the product in eq 11 would be a radical cation. In our initial communication we suggested that

$$Ru(dppe)(CO)_3 + ArNO_2 \rightarrow [Ru(dppe)(CO)_3^{\bullet+}ArNO_2^{\bullet-}] \quad (11)$$

$[Ru(dppe)(CO)_3]^+$ might be the species observed in the high-pressure FTIR spectral study. Subsequent research established[60] that these radical cations are too short-lived even at low temperature to account for the spectrum of the catalytic solutions. These studies on the chemical and electrochemical oxidation of the series of complexes $Ru(PR_3)_2(CO)_3$ (R = Ph, Cy, and Bz) and $Ru(dppe)(CO)_3$ did establish, however, the viability of $[Ru(dppe)(CO)_3]^+$ as an intermediate in the catalysis. In all cases the radical cation $[Ru(PR_3)_2(CO)_3]^+$ could be formed at low temperatures and spectrally characterized or trapped by a suitable reagent. Several observations from the study of these radical cations are relevant to this catalytic study. Once formed the radical cations were very reactive (substantially more reactive than the corresponding iron compounds). The reactivity was dependent on the structure with the radical cation of $Ru(dppe)(CO)_3$ being the most reactive. Finally, cyclic voltammetry established the reversible nature of the oxidation of $Ru(PR_3)_2(CO)_3$. The $E_{1/2}$ values showed the trend of increasing ease of oxidation with increasing electron-donating ability of the phosphine. With $Ru(dppe)(CO)_3$, however, the oxidation was irreversible which unfortunately precludes a direct comparison of $E_{1/2}$ values. The oxidation wave was 300 mV more negative than the value for $Ru(PPh_3)_2(CO)_3$, a trend also found in the comparison between $Fe(PPh_3)_2(CO)_3$ and $Fe(dppe)(CO)_3$, It is noteworthy that while $Ru(dppe)(CO)_3$ reacts with nitroaromatics at room temperature, $Ru(PPh_3)_2(CO)_3$ does not.

Scheme II shows a series of reactions that could occur following the electron-transfer step. Radical recombination could occur by nucleophilic attack on the cationic metal carbonyl which would

(56) Deno, N. C.; Gaugler, R. W.; Schulze, T. J. *J. Org. Chem.* **1966**, *31*, 1968.
(57) Hurlburt, P. K.; Kellett, P. J.; Anderson, O. P.; Strauss, S. H. *J. Chem. Soc., Chem. Commun.* **1990**, 576.
(58) Crabtree, R. H.; Davis, M. W.; Mellea, M. F.; Mihelcic, J. M. *Inorg. Chim. Acta* **1983**, *72*, 223.
(59) Berman, R. S.; Kochi, J. K. *Inorg. Chem.* **1980**, *19*, 248.
(60) Sherlock, S. J.; Boyd, D. C.; Moasser, B.; Gladfelter, W. L. *Inorg. Chem.* **1991**, *30*, 3626.

**Scheme II.** Phase 1: First Deoxygenation

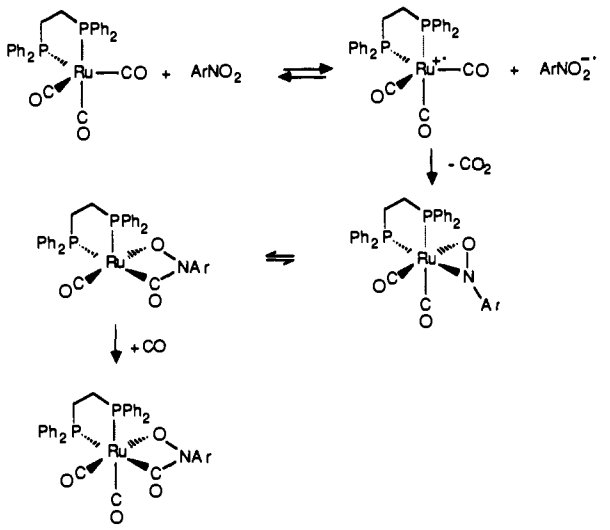

set the stage for the expulsion of $CO_2$ by a migratory deinsertion of the ArNO. The final formation of the first isolable species could result from the insertion of CO into an $\eta^2$-ArNO ligand. Although the CO insertion into the nitrosoarene group is unprecedented, Cenini and co-workers have observed the insertion of alkynes as shown in eq 12.[61] Note that the insertion also occurs into the

$$Pt(PPh_3)_2(\eta^2\text{-PhNO}) + MeO(O)CC{\equiv}CC(O)OMe \longrightarrow$$

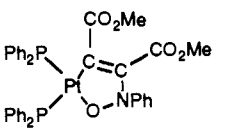

(12)

metal–nitrogen bond. All attempts to intercept the analogous $\eta^2$-ArNO ruthenium intermediate have been unsuccessful.

**Phase 2: Second Deoxygenation and Aniline Formation.** One possible mechanism for the cleavage of the second N–O bond involves reversing the last two steps shown in Scheme II to reform a nitrosoarene complex.[40] From this intermediate, insertion of CO into the Ru–O bond could lead to the species shown in II′ (eq 13) which could eliminate $CO_2$ yielding a phenylimido ligand (eq 14). The intermediate $Ru(dppe)(CO)_2[C(O)N(Ar)O]$,

$$Ru(dppe)(CO)_2(ArNO) + CO \rightarrow Ru(dppe)(CO)_2[C(O)ON(Ar)] \quad (13)$$
$$\text{II}'$$

$$\text{II}' \rightarrow CO_2 + Ru(dppe)(CO)_2(NAr) \quad (14)$$

however, is thermally stable to 60 °C and undergoes no further reaction in aprotic solvents even under an atmosphere of CO. In addition, no exchange of any of the carbonyl groups was observed after a solution of $Ru(dppe)(CO)_2[C(O)N(Ar)O]$ under $^{13}CO$ was stirred for 3 days at 25 °C. If the last two steps shown in Scheme II were reversible under these conditions, exchange would have been observed. These results suggest a different mechanism must be operating.

It is at this point in the catalysis that the presence of methanol is critical. Equation 15 summarizes the products observed during the reaction of $Ru(dppe)(CO)_2[C(O)N(Ar)O]$ with methanol under a CO atmosphere at 70 °C. If the temperature is lowered

$$Ru(dppe)(CO)_2[C(O)N(Ar)O] + MeOH + CO \rightarrow Ru(dppe)(CO)_2[C(O)OMe]_2 + Ru(dppe)(CO)_3 + CO_2 + ArNH_2 \quad (15)$$

to room temperature, little of the reduced complex, $Ru(dppe)(CO)_3$, is formed and a new intermediate formulated as $Ru(dppe)(CO)_2(OMe)_2$ is observed (eq 16). The reaction of $Ru(dppe)(CO)_2[C(O)N(Ar)O]$ with HCl (eq 17) shows an identical product distribution to that found in eq 16, suggesting that methanol is also reacting as a Brönsted acid.

$$Ru(dppe)(CO)_2[C(O)N(Ar)O] + MeOH \rightarrow Ru(dppe)(CO)_2(OMe)_2 + CO_2 + ArNH_2 \quad (16)$$

$$Ru(dppe)(CO)_2[C(O)N(Ar)O] + HCl \rightarrow Ru(dppe)(CO)_2Cl_2 + CO_2 + ArNH_2 \quad (17)$$

The following drawing shows the three sites on $Ru(dppe)(CO)_2[C(O)N(Ar)O]$ that are likely to be the most basic. Protonation may induce a migratory insertion of CO into the Ru–O bond to create an incipient $CO_2$; however, no experimental details address this mechanism.

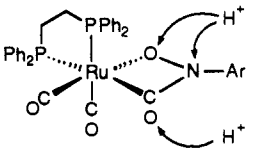

The formation of the bis(methoxycarbonyl) complex (the second part of eq 15) involves the insertion of CO into the two Ru–OMe bonds. For the low-valent, later transition elements, the insertion of CO into the metal–heteroatom (usually $^-OR$ or $^-NR_2$) bonds can occur via an intramolecular mechanism (similar to most insertions into metal-alkyl bonds) or a mechanism that involves initial dissociation of the $^-OR$ or $^-NR_2$ ligand.[62] In the latter case, coordination of the CO to the vacant site would be followed by nucleophilic attack on this electrophilic center. Differentiating between these two has proven to be difficult with other metal complexes, and thus far we have no evidence ruling out either process.

As shown in eq 15 a minor portion of the metal is reduced to the zerovalent starting material without the formation of any carbamate. A reasonable explanation for this product also starts with $Ru(dppe)(CO)_2(OMe)_2$, and the overall stoichiometry is shown in eq 18. This reaction could begin with dissociation of

$$Ru(dppe)(CO)_2(OMe)_2 + CO \rightarrow H_2CO + MeOH + Ru(dppe)(CO)_3 \quad (18)$$

one of the methoxide ligands (eq 19) followed by a $\beta$-hydrogen elimination from the remaining methoxide (eq 20). Deprotonation

$$Ru(dppe)(CO)_2(OMe)_2 \rightarrow MeO^- + [Ru(dppe)(CO)_2(OMe)]^+ \quad (19)$$

$$[Ru(dppe)(CO)_2(OMe)]^+ \rightarrow [Ru(dppe)(CO)_2(H_2C{=}O)H]^+ \quad (20)$$

of this product would produce a neutral formaldehyde complex which could lead to $Ru(dppe)(CO)_3$ following substitution of $H_2CO$ with CO (eq 21). Although formaldehyde itself is not

$$[Ru(dppe)(CO)_2(H_2C{=}O)H]^+ + MeO^- + CO \rightarrow H_2CO + MeOH + Ru(dppe)(CO)_3 \quad (21)$$

isolated during the catalysis, the Schiff base formed from the condensation of formaldehyde with aniline is observed in reactions involving high initial concentrations of aniline.

**Phase 3: Carbamate Formation.** The final stage of the reaction involves the formation of carbamate by the reaction of aniline with the bis(methoxycarbonyl) complex (eq 22). The intermediacy of carboalkoxy complexes in related reactions has been reviewed.[63]

$$Ru(dppe)(CO)_2[C(O)OMe]_2 + ArNH_2 \rightarrow ArNHC(O)OMe + MeOH + Ru(dppe)(CO)_3 \quad (22)$$

Although the overall stoichiometry is known, details of the mechanism are not. The critical product-forming step could result from reactions such as the direct nucleophilic attack of aniline

(61) Cenini, S.; Porta, F.; Pizzotti, M.; La Monica, G. *J. Chem. Soc., Dalton Trans.* **1984**, 355.

(62) Bryndza, H. E.; Tam, W. *Chem. Rev.* **1988**, *88*, 1163.
(63) Milstein, D. *Acc. Chem. Res.* **1988**, *21*, 428–434.

**Scheme III.** Aniline, Methanol, and CO Interconversions on $Ru(dppe)(CO)_2([Ru])$

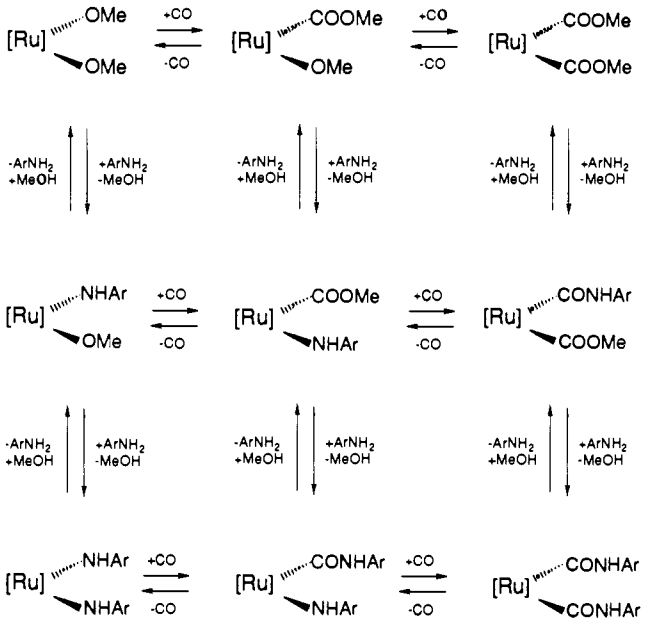


on the methoxycarbonyl ligand of $Ru(dppe)(CO)_2[C(O)OMe]_2$ or by the reductive elimination from an intermediate such as those shown below.

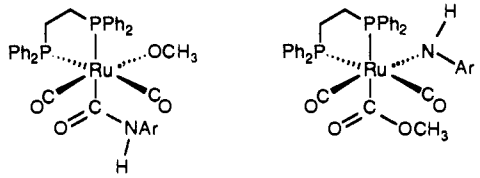


The interconversion between the methoxycarbonyl and carbamoyl ligands could involve direct attack on the coordinated ligand by the uncomplexed nucleophile or a separate set of migratory deinsertion and insertion reactions. The multitude of possible products is best represented by the matrix shown in Scheme III. From left to right the molecules are related by the addition of CO whereas the progression from top to bottom involves exchange of an $ArNH^-$ for a $MeO^-$. This matrix does not represent specific mechanisms, rather it outlines the stoichiometries of a series of closely related chemical transformations. We have experimental evidence for the species in the first and third columns of row 1. On the basis of closely related literature precedent, we would expect that the aniline/methanol exchange down column 1 should be facile.[64] There is precedent for the substitution of amines for alkoxo groups of alkoxycarbonyl ligands[65] that could lead to the structures shown above.

Consideration of this matrix of intermediates leads to three important points. First, the matrix represents a family of complexes whose individual energies and chemical reactivities probably differ little from each other within a given column. Second, the actual pathway leading from the bis(methanolato) or bis(methoxycarbonyl) complexes to the carbamate may be highly dependent on the conditions, especially the CO pressure and the concentration of aniline. Third, at high aniline concentrations the relative abundance of species in the lower right of the matrix should increase. Experimentally, under these conditions we observe the formation of diarylurea.

**In Situ FTIR Spectroscopy.** The highlight of the spectral changes shown in Figure 8 is the formation of a new intermediate having two prominent absorptions of approximately equal intensity at 2053 and 2000 $cm^{-1}$. The match between these peaks and those found for pure samples of $Ru(dppe)(CO)_2[C(O)OMe]_2$ suggests that the latter complex is the predominant species present during the actual catalysis. Corroborating evidence for the presence of $Ru(dppe)(CO)_2[C(O)OMe]_2$ during the catalytic reaction comes from the $^{31}P$ NMR spectrum of a sample that was rapidly quenched from the high-temperature and high-pressure conditions. Figure 9 shows that $Ru(dppe)(CO)_2[C(O)OMe]_2$ is the major species present. This evidence is critical for knowing where to begin the kinetic analysis of the catalysis.

**Overall Kinetics of the Catalysis.** The experimentally derived kinetic model for the catalysis is shown in eqs 5 and 6. Solution of these equations has proven to give satisfactory fits to the experimental results within the concentration ranges studied. Deviations from this model were observed only when large quantities of aniline were added to the starting solution. As stated above, diarylurea crystallization was noted under these conditions and led to significant deviations in the mass balance during the catalysis. Under such conditions the rate of methanolysis of the urea may be the rate-determining step in carbamate production.

The overall kinetics will not allow us to differentiate among the many possible detailed pathways which yield carbamate. It is valuable, however, to consider at least one scenario, as shown in eqs 23–26, that ties together the catalytic kinetics, the in situ spectroscopy, and the stoichiometric reactions. One of the kinetically significant events involve a second-order reaction with aniline to produce carbamate and regenerate the starting catalyst. Equation 27 is the expression for this step. The shunt that allows regeneration of $Ru(dppe)(CO)_3$ without carbamate formation would begin with CO dissociation followed by deinsertion of the OMe ligand. This portion of the catalysis is measured by the rate of aniline formation and is described by eq 28. According to the mass balance of the reaction, the sum of eqs 27 and 28 equals the rate of disappearance of the nitroaromatic. It is clear that this mechanism reduces to the experimentally derived equation (eq 29) providing that $k_{-1}[CO] > k_2$.

$$Ru(dppe)(CO)_2[C(O)OMe]_2 \underset{k_{-1}}{\overset{k_1}{\rightleftharpoons}} CO + Ru(dppe)(CO)[C(O)OMe]_2 \quad (23)$$

$$Ru(dppe)(CO)[C(O)OMe]_2 \xrightarrow{k_2} CH_3OH + H_2CO + Ru(dppe)(CO)_3 \quad (24)$$

$$Ru(dppe)(CO)_2[C(O)OMe]_2 + ArNH_2 \xrightarrow{k_3} Ru(dppe)(CO)_3 + CH_3OH + ArNHC(O)OCH_3 \quad (25)$$

$$Ru(dppe)(CO)_3 + ArNO_2 + 2CH_3OH + 3CO \xrightarrow{fast} ArNH_2 + 2CO_2 + Ru(dppe)(CO)_2[C(O)OMe]_2 \quad (26)$$

$$d[Carb]/dt = k_3[ArNH_2]\{Ru(dppe)(CO)_2[C(O)OMe]_2\} \quad (27)$$

$$d[ArNH_2]/dt = k_1k_2\{Ru(dppe)(CO)_2[C(O)OMe]_2\}/\{k_2 + k_{-1}(p_{CO})\} \quad (28)$$

$$-d[ArNO_2]/dt = k_{a(obs)}[Ru]/p_{CO} + k_{c(obs)}[Ru][ArNH_2] \quad (29)$$

**Requirements for the Catalyst and Relationship among the Published Catalysts.** One of the salient features of the metal complex in this catalytic reaction is its ability to shuttle between zero and divalent ruthenium. The facile interconversion between $d^8$ and $d^6$ complexes is important in many homogeneous catalytic reactions.[66] Because the initial substrate activation event involves reduction of the nitroaromatic, ruthenium(0) may be best suited due to its relatively lower reduction potential compared to related $d^8$ complexes of rhodium(I) or palladium(II), both of which have been reported to catalyze the carbonylation of nitroaromatics. Palladium, in particular, has been the most common metal used in the carbonylations to give isocyanates directly.[1] Unfortunately it suffers from the propensity to precipitate inactive palladium

(64) Bryndza, H. E.; Fong, L. K.; Paciello, R. A.; Tam, W.; Bercaw, J. E. *J. Am. Chem. Soc.* **1987**, *109*, 1444.
(65) Angelici, R. J. *Acc. Chem. Res.* **1972**, *5*, 335.
(66) Parshall, G. W. *Homogeneous Catalysis*; Wiley: New York, 1980.

metal under reducing conditions (such as a CO atmosphere).

The rate-determining step in the carbonylation catalyzed by $Ru(dppe)(CO)_3$ involves a second-order reaction between aniline and $Ru(dppe)(CO)_2[C(O)OMe]_2$. As discussed above, nucleophilic attack of the amine on the coordinated methoxycarbonyl ligand could be the responsible mechanism. We would predict that making the phosphorus ligand smaller in cone angle and less electron donating would increase the activity of the catalyst. Converting the two phosphorus donors back to carbonyl ligands would accomplish this. $Ru(CO)_5$ can be prepared in situ from $Ru_3(CO)_{12}$ under high CO pressure. It is interesting, however, that the rate of the catalytic reaction is significantly slower when compared to that of $Ru(dppe)(CO)_3$.[12,13] Other, as yet unidentified, factors may be contributing to the mechanism of catalysis using $Ru_3(CO)_{12}$.

One of the shortcomings of all of the catalytic systems for nitroaromatic carbonylations is their difficulty in carbonylating completely dinitroaromatic substrates, such as 2,4-dinitrotoluene.[1] Consideration of the rate-determining step in the $Ru(dppe)(CO)_3$ catalytic system reveals some insight into this problem. The substrate would have to proceed around the cycle two times for complete carbonylation. After the first nitro group is reduced, the resulting nitroaminotoluene would have significantly reduced nucleophilicity and thus may proceed sluggishly through the carbamate-forming stage. This would allow the catalyst sufficient time to cycle back through the shunt to $Ru(dppe)(CO)_3$. Because it is a strong oxidant, all of the dinitroaromatic would be reduced before the catalyst would attempt to reduce the intermediate nitroaminotoluene. The presence of the very strong electron donating amino substituent may make the further reduction of nitroaminotoluene the slow step in the reaction.

The detailed studies described here for $Ru(dppe)(CO)_3$ confirm that the kinetics of catalysis are similar to those found for $Ru_3(CO)_{12}$.[11-14] Although Grate and co-workers noted similarities in the kinetics among several of the ruthenium complexes tested,[54] all ruthenium carbonyl catalysts do not exhibit the same behavior. The recently reported catalytic activity[67] of the dinuclear complex, $Ru_2(dmpm)_2(CO)_5$, was found to be independent of the concentration of aniline.

(67) Gargulak, J. D.; Hoffman, R. D.; Gladfelter, W. L. *J. Mol. Catal.* **1991**, *68*, 289.

## Conclusions

Using a combination of in situ spectroscopic analysis, chemical kinetics, and studies of stoichiometric transformations, we have provided the first experimentally supported mechanistic picture of the homogeneous catalytic carbonylation of nitroaromatics. The studies of $Ru(dppe)(CO)_3$ revealed that the catalysis can be broken into three distinct phases each proceeding with a correspondingly higher kinetic barrier. The initial interaction between the catalyst and substrate is proposed to involve a single electron transfer. The first observable intermediate contains a new organometallic functional group that was found to react with the protons of methanol in the second stage of the catalysis. At this point free aniline is produced. One of the interesting aspects of this mechanism is that it avoids invoking a metal-complexed arylnitrene (arylimido) intermediate. The metal-containing species present at the end of phase 2 is $Ru(dppe)(CO)_2[C(O)OMe]_2$, which is also the species observed by FTIR spectroscopy during the catalytic reaction. The rate-determining step for carbamate formation involves the reaction of $Ru(dppe)(CO)_2[C(O)OMe]_2$ with aniline. Direct reduction of $Ru(dppe)(CO)_2[C(O)OMe]_2$ back to $Ru(dppe)(CO)_3$ is inhibited by CO. This proposal not only explains the mechanism of carbamate formation but also offers a quantitative explanation for the selectivity of the catalytic reaction.

Further kinetic studies are in progress to establish the details of the reaction between $Ru(dppe)(CO)_2[C(O)OMe]_2$ and aniline. Ultimately we hope to be able to compare the kinetics of the stoichiometric reactions to those of the catalytic reaction described in this publication.

**Acknowledgment.** This research was sponsored by grants from the Amoco Chemical Corp. and National Science Foundation. We gratefully acknowledge the valuable interaction with John Grate and David Hamm.

**Supplementary Material Available:** Tables of atomic and hydrogen atom positions and thermal parameters (9 pages); listing of structure factors (33 pages). Ordering information is given on any current masthead page.